Article
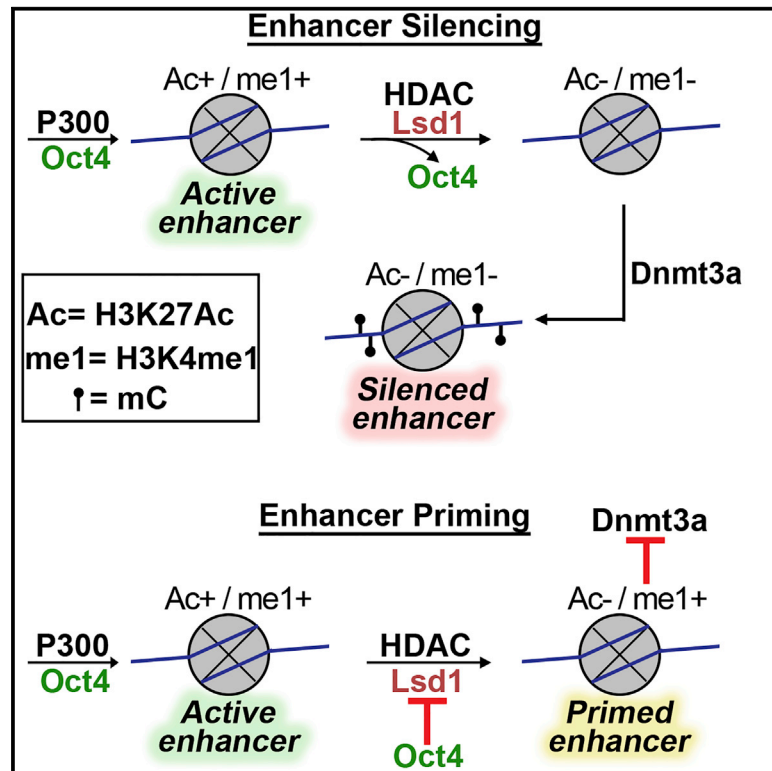
Oct4-Mediated Inhibition of Lsd1 Activity Promotes the Active and Primed State of Pluripotency Enhancers

Graphical Abstract

Authors

Lama AlAbdi, Debapriya Saha, Ming He, ..., James A. Breedlove, Nadia A. Lanman, Humaira Gowher

Correspondence

hgowher@purdue.edu

In Brief

AlAbdi et al. show that aberrant expression of Oct4 in cancer stem cells can facilitate the establishment of the "primed" enhancer state of pluripotency genes. Reactivation of these enhancers would support tumorigenicity.

Highlights

- Pluripotency genes are partially repressed in F9 ECCs post-differentiation

- Oct4 interacts with Lsd1 and inhibits its histone demethylation activity

- Inhibition of Lsd1 by Oct4 leads to retention of H3K4me1 at pluripotency gene enhancers

- Retention of H3K4me1 inhibits DNA methylation leading to the "primed" enhancer state

CellPress

Oct4-Mediated Inhibition of Lsd1 Activity Promotes the Active and Primed State of Pluripotency Enhancers

Lama AlAbdi,[1] Debapriya Saha,[1] Ming He,[1] Mohd Saleem Dar,[1] Sagar M. Utturkar,[2] Putu Ayu Sudyanti,[3] Stephen McCune,[1] Brice H. Spears,[1] James A. Breedlove,[1] Nadia A. Lanman,[2,4] and Humaira Gowher[1,2,5,*]
[1]Department of Biochemistry, Purdue University, West Lafayette, IN 47907, USA
[2]Purdue University Center for Cancer Research, Purdue University, West Lafayette, IN 47907, USA
[3]Department of Statistics, Purdue University, West Lafayette, IN 47907, USA
[4]Department of Comparative Pathobiology, Purdue University, West Lafayette, IN 47907, USA
[5]Lead Contact
*Correspondence: hgowher@purdue.edu
https://doi.org/10.1016/j.celrep.2019.11.040

SUMMARY

An aberrant increase in pluripotency gene (PpG) expression due to enhancer reactivation could induce stemness and enhance the tumorigenicity of cancer stem cells. Silencing of PpG enhancers (PpGe) during embryonic stem cell differentiation involves Lsd1-mediated H3K4me1 demethylation and DNA methylation. Here, we observed retention of H3K4me1 and DNA hypomethylation at PpGe associated with a partial repression of PpGs in F9 embryonal carcinoma cells (ECCs) post-differentiation. H3K4me1 demethylation in F9 ECCs could not be rescued by Lsd1 overexpression. Given our observation that H3K4me1 demethylation is accompanied by strong Oct4 repression in P19 ECCs, we tested if Oct4 interaction with Lsd1 affects its catalytic activity. Our data show a dose-dependent inhibition of Lsd1 activity by Oct4 and retention of H3K4me1 at PpGe in Oct4-overexpressing P19 ECCs. These data suggest that Lsd1-Oct4 interaction in cancer stem cells could establish a "primed" enhancer state that is susceptible to reactivation, leading to aberrant PpG expression.

INTRODUCTION

Cell-type-specific gene expression is regulated by chromatin conformation, which facilitates the interaction of distally placed enhancer elements with the specific gene promoter (Banerji et al., 1981; Bulger and Groudine, 2011; Ong and Corces, 2011; Plank and Dean, 2014). Enhancers house the majority of transcription factor binding sites and amplify basal transcription, thus playing a critical role in signal-dependent transcriptional responses (summarized in Heinz et al., 2015). Epigenome profiling combined with the transcriptional activity in various cell types led to identification of potential enhancers, which are annotated as silent, primed, or active based on their epigenetic features. These epigenetic features include histone modifica-

tions and DNA methylation (Ernst and Kellis, 2010; Ernst et al., 2011; Calo and Wysocka, 2013). Whereas histone H3K4me1 (monomethylation) and H3K4me2 (dimethylation) is present at both active and primed enhancers, active enhancers invariantly are marked by histone H3K27Ac (acetylation) and/or transcribed to produce enhancer RNA (eRNA) (Heintzman et al., 2007; Heinz et al., 2010; Rada-Iglesias et al., 2011; Creyghton et al., 2010; Zentner et al., 2011; Zhu et al., 2013b).

During embryonic stem cell (ESC) differentiation, pluripotency gene (PpG)-specific enhancers are silenced via changes in histone modifications and a gain of DNA methylation (Whyte et al., 2012; Mendenhall et al., 2013; Petell et al., 2016). In response to the differentiation signal, the coactivator complex (Oct4, Sox2, Nanog, and mediator complex) dissociates from the enhancer, followed by the activation of pre-bound Lsd1-Mi2/NuRD enzymes. The histone demethylase Lsd1 demethylates H3K4me1, and the HDAC activity of the NuRD (Nucleosome Remodeling Deacetylase) complex deacetylates H3K27Ac (Whyte et al., 2012). Our previous studies have shown that the histone demethylation event is critical for the activation of DNA methyltransferase Dnmt3a, which interacts with the demethylated histone H3 tails through its chromatin-interacting ADD (ATRX-Dnmt3a-Dnmt3L) domain, allowing site-specific methylation at PpG enhancers (PpGe) (Petell et al., 2016). These findings were further supported by biochemical studies showing that the Dnmt3a-ADD domain interacts with the histone H3 tail and this interaction is inhibited by H3K4 methylation (Guo et al., 2015; Li et al., 2011a; Ooi et al., 2007; Otani et al., 2009), which suggest that aberrant inhibition of Lsd1 demethylase activity could cause a failure to gain DNA methylation, leading to incomplete repression of PpGs.

Several studies have reported on potential mechanisms that control site-specific targeting and catalytic activity of Lsd1. Whereas Lsd1 interaction with CoREST (corepressor of REST, an RE1 silencing transcription factor/neural restrictive silencing factor) activates the enzyme, BHC80 inhibits Lsd1 demethylation activity (Shi et al., 2005). The substrate specificity of Lsd1 is regulated by its interaction with androgen receptor and estrogen-related receptor α or by alternative splicing, which adds four or eight amino acids to the Lsd1 enzyme (Carnesecchi et al., 2017; Metzger et al., 2005; Laurent et al., 2015; Zibetti

et al., 2010; Wang et al., 2015a). Lsd1 is targeted to various genomic regions through its interaction with SNAG domain-containing transcription factors (TFs), such as Snail and GFI1B (McClellan et al., 2019; Vinyard et al., 2019). The SNAG domain binds to the active site of Lsd1 by mimicking the histone H3 tail and could potentially inhibit its activity (Baron et al., 2011). Interaction of the p53 C' terminal domain with the Lsd1 active site inhibits Lsd1 enzymatic activity (Speranzini et al., 2017). Lsd1 was also shown to be present in the Oct4 interaction network, and therefore could be targeted to Oct4-bound regulatory elements, which largely control pluripotency and stemness (van den Berg et al., 2010; Pardo et al., 2010; Ding et al., 2012).

Studies by the Cancer Genome Anatomy Project (CGAP) show that one out of three cancers express PpGs, suggesting their role in dysregulated proliferation during tumorigenesis (Zhang et al., 2013; Liu et al., 2013). Further, expression of PpGs, *Oct4*, *Sox2*, and *Nanog* potentiates self-renewal of putative cancer stem cells (CSCs) (Ben-Porath et al., 2008; Feske, 2007; Linn et al., 2010; Peng et al., 2010; Kumar et al., 2012; Wang et al., 2013; Mak et al., 2012; Wen et al., 2010; Jeter et al., 2011). CSCs proliferate as well as differentiate to give rise to cancer cells of various lineages (Iglesias et al., 2017). However, to retain the ability to proliferate, many cancer cells maintain expression of PpGs (Gwak et al., 2017; Yang et al., 2018). This has led to the development of terminal differentiation therapy, which aims to limit the proliferating cancer cell population (de Thé, 2018). Embryonal carcinoma cells (ECCs) have been used as a model cell line to study CSCs. ECCs were derived from developing mouse embryos at embryonic days (E)6–7.5 and share regulatory characteristics with ESCs, including their ability to differentiate into various somatic lineages (Alonso et al., 1991; Han et al., 2017; Andrews et al., 2005; Zhu et al., 2013a). To understand the mechanism by which cancer cells retain PpG expression, we investigated the mechanism of enhancer-mediated regulation of PpG expression in ECCs. Our data showed that, in differentiating F9 ECCs, the PpGs are only partially repressed. This was concomitant with H3K27 deacetylation, but with an absence of Lsd1-mediated H3K4me1 demethylation at PpGe. The presence of H3K4me1 prevented Dnmt3a from methylating the DNA at these sites, potentially abrogating PpGe silencing. Drug-mediated inhibition as well as overexpression of Lsd1 had little or no effect on enhancer silencing and PpG repression, confirming an absence of Lsd1 dependence in differentiating ECCs. Given that Oct4 was expressed at substantial levels in F9 ECCs post-differentiation, we investigated the effect of Lsd1-Oct4 interaction on Lsd1 catalytic activity. Using *in vitro* histone demethylation assays, we discovered that Lsd1-Oct4 interaction inhibits Lsd1 activity, which could potentially result in the retention of H3K4me1 at PpGe in F9 ECCs. We tested this prediction in P19 ECCs, in which Oct4 expression is strongly reduced post-differentiation and H3K4me1 is demethylated at PpGe. The observation that overexpression of Oct4 in differentiating P19 ECCs led to retention of H3K4me1 at PpGe confirmed the role of Oct4-mediated Lsd1 inhibition at these sites. Taken together, our data show that inhibition of Lsd1 activity and Dnmt3a leads to the establishment of a "primed" enhancer state, which is open for coactivator binding and prone to reactivation. We spec-

ulate that aberrant expression of Oct4 in CSCs facilitates the establishment of "primed" enhancers, the reactivation of which supports tumorigenicity.

RESULTS

PpGs Are Partially Repressed in Differentiating F9 ECCs

ECCs share many characteristics with ESCs, including mechanisms governing regulation of gene expression and differentiation (Alonso et al., 1991). Based on the observation that aberrant PpG expression is commonly found in cancers (Zhang et al., 2013; Liu et al., 2013), we compared the magnitude of PpG repression in F9 ECCs with that in ESCs pre- and post-differentiation. ESCs and F9 ECCs were induced to differentiate with retinoic acid (RA), and expression of a subset of PpGs at 4 days (D4) post-induction was measured by qRT-PCR. In ESCs, the expression of most PpGs was reduced by more than 80% post-differentiation. The expression of *Sox2* and *Trim28* was maintained as an anticipated response to RA signaling guiding ESCs toward neural lineage (Figure 1A). However, in differentiating F9 ECCs, several PpGs were incompletely repressed, of which genes encoding the pioneer factors Oct4 showed a 75% loss of expression while Nanog remain unchanged. A substantial increase in the expression of the genes *Lefty1* and *Lefty2* in F9 ECCs suggests potential transient activation of germ cell and testis developmental programs (Zhu et al., 2013a) (Figure 1B). To ensure that incomplete repression of PpGs was not the consequence of delayed response to RA signaling, we cultured cells for 8 days (D8). A variable decrease in PpGs was observed in the range of 25%–75%, with the highest repression in *Lefty 2* (Figure 1B). Positive alkaline phosphatase staining and SSEA-1 immunofluorescence, that is completely lost in ESCs post-differentiation, is retained in differentiating F9 ECCs, providing additional evidence for the expression of PpGs in these cells (Figures 1C and 1D). We asked if failure to exit pluripotency in F9 ECCs was caused by an inability to activate lineage-specific genes. Our data showed a 5- to 60-fold increase in the expression of the lineage specific genes *Gata4*, *Foxa2*, *Olig2*, *Gata6*, *Cxcr4*, and *Fgf5* (Figure 1E), reflecting a standard response to differentiation signal. Given that previous studies in ESCs have established a critical role of enhancer silencing incomplete PpG repression, we next investigated if PpGe were fully decommissioned in F9 ECCs post-differentiation (Petell et al., 2016).

DNA Methylation Is Not Established at PpGe during F9 ECC Differentiation

In differentiating ESCs, PpGe silencing involves gain of DNA methylation, which is required for complete PpG repression (Petell et al., 2016). We used bisulfite sequencing (Bis-seq) to compare DNA methylation changes at a subset of PpGe in F9 ECCs to that in ESCs post-differentiation. Whereas DNA methylation was significantly increased at most PpGe in ESCs D4 post-differentiation, these sites remained hypomethylated (<10% methylation; Tierling et al., 2018) in F9 ECCs (Figures 2A and 2B). A similar hypomethylated state persisted at PpG promoters in F9 ECCs, except the highly methylated *Lefty2* promoter, where DNA methylation was partially lost post-differentiation (Figure S1A). This result is consistent with the
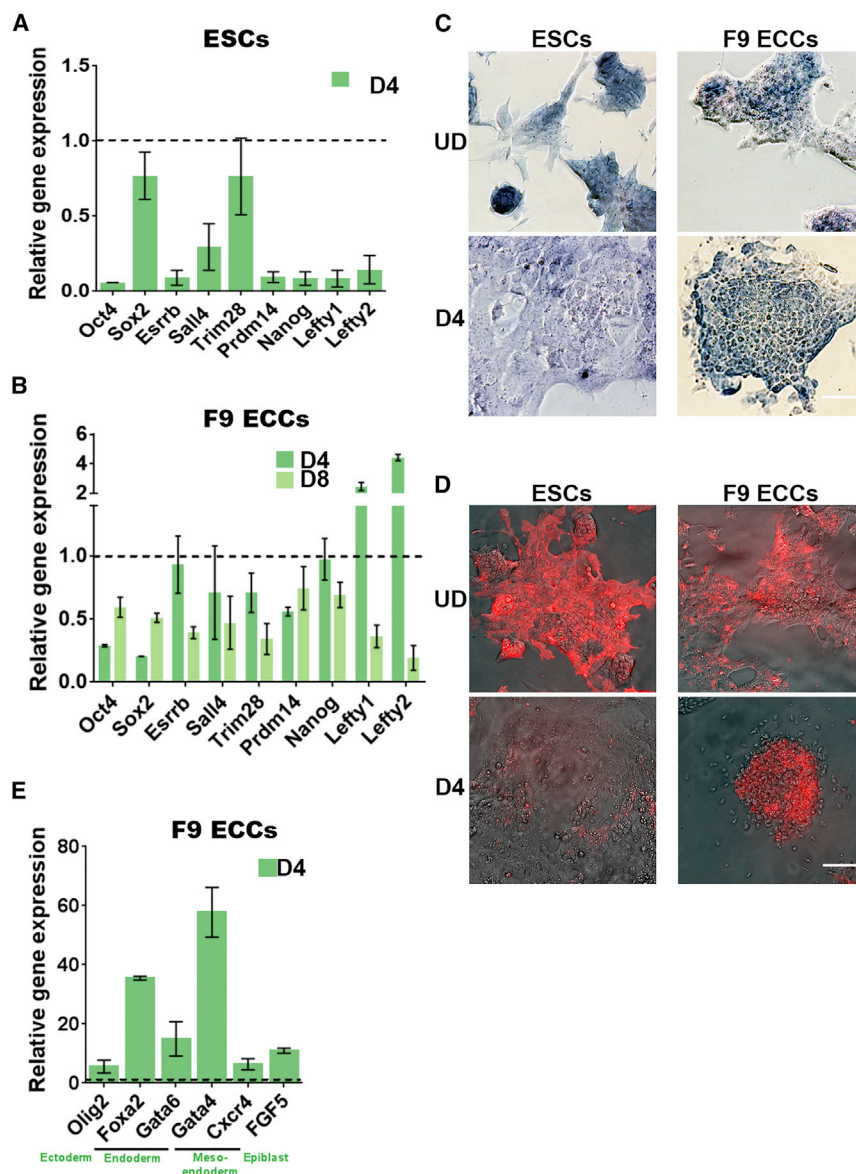
Figure 1. Pluripotency Genes Are Partially Repressed in Embryonal Carcinoma Cells

(A, B, and E) Gene expression analysis by qRT-PCR of PpGs in (A) F9 ESCs, (B) ECCs, and (E) lineage-specific genes in F9 ECCs. The threshold cycle (C_t) values for each gene were normalized to *Gapdh*, and expression is shown relative to that in undifferentiated cells (dotted line). In F9 ECCs, the lineage-specific genes show a 5- to 60-fold induction of gene expression (E), whereas the expression of PpGs is, on average, reduced to about 50% post-differentiation (B). Average and SEM of two biological replicates are shown for each gene.

(C and D) Alkaline phosphatase staining (C) and SSEA-1 immunofluorescence (D) of ESCs and F9 ECCs pre- and post-differentiation. A positive signal indicates pluripotency that is lost post-differentiation in ESCs. Scale bars, 100 μm.

UD, undifferentiated; D4 and D8, days post-induction of differentiation; ESCs, embryonic stem cells; F9 ECCs, F9 embryonal carcinoma cells; PpGs, pluripotency genes.

We anticipated that the DNA methylation established by transiently overexpressing Dnmt3a would be maintained by Dnmt1 during multiple cell divisions (Lyko, 2018). To ensure the detection of methylation established by recombinant Dnmt3a, we differentiated the cells for D8. However, DNA methylation levels at PpGe except Oct4 (15%) were well below 10%, which is within the range of detection error by this method (Tierling et al., 2018). A small gain within this range was observed, suggesting a spurious low methylation during cell divisions (Figure 2C). 5 out of 8 PpGs showed no additional decrease in expression (p > 0.1) when compared to untransfected differentiated cells (Figure 2D), indicating that overexpression of Dnmt3a is unable to rescue the differentiation defects observed in F9 ECCs. The absence of complete PpG repression concomitant with little or no significant gain in DNA methylation at PpGe predicts a potential disruption in the mechanism that mediates PpGe decommissioning.

We performed MethylRAD sequencing to determine the extent of DNA methylation defect and to analyze changes in DNA methylation at all PpGe in F9 ECCs pre- and post-differentiation (Wang et al., 2015b). This method uses an *Fsp*EI restriction enzyme, which cuts DNA bidirectionally from mC to create 31–32 bp fragments (Cohen-Karni et al., 2011; Zheng et al., 2010). The restriction fragments were isolated for library preparation and high-throughput sequencing. Using this method, we captured DNA methylation at 1,370,254 cytosines genome-wide. The reads were distributed among all chromosomes representing all annotated genomic elements (Figure S2A). DNA methylation levels at

observed partial repression of most PpGs and an induction of *Lefty2* expression in these cells (Figure 1B). Furthermore, in ESCs, gain of DNA methylation at *Trim28* and *Sox2* enhancers suggests enhancer-switching, which involves a potential use of neural lineage specific enhancers to maintain a high expression of these genes post-differentiation (Figures 1A and 2A).

We confirmed that absence of DNA methylation at PpGe was not due to low expression of Dnmt3a in F9 ECCs post-differentiation (Figures S1B and S1C). Based on previous observations in cancers that overexpression of DNA methyltransferases leads to DNA hypermethylation (Yu et al., 2015b; Gao et al., 2015; Ma et al., 2018; Jones et al., 2016; Schübeler, 2015), we tested if overexpression of Dnmt3a could rescue DNA methylation at PpGe. F9 ECCs were transfected with Myc-Dnmt3a and differentiated at 24 h post-transfection to ensure expression of recombinant Dnmt3a during early differentiation (Figure S1D).
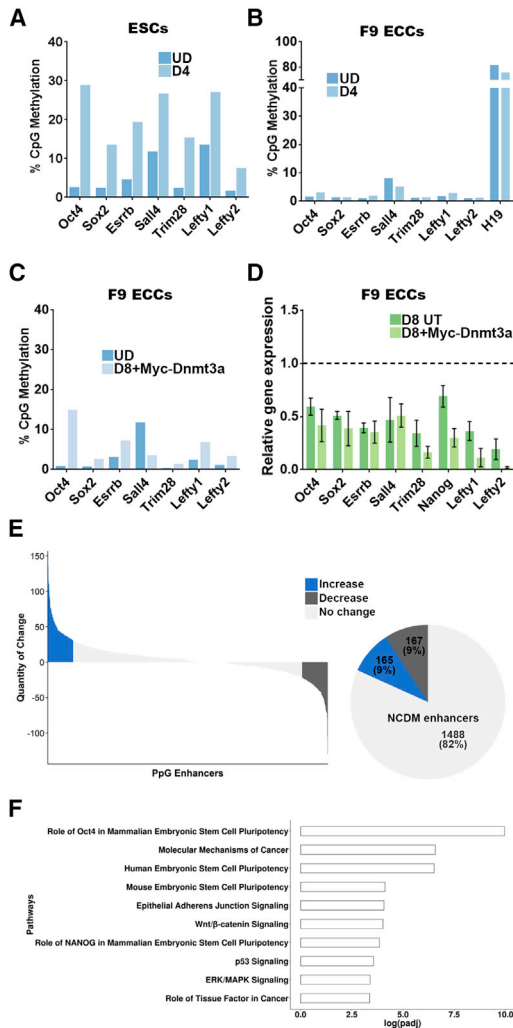
Figure 2. Pluripotency Gene Enhancers Do Not Gain DNA Methylation in Embryonal Carcinoma Cells

(A–C) DNA methylation analysis using Bis-seq. Genomic DNA was treated with bisulfite and PpGe regions were amplified by PCR. The amplicons were sequenced on a high-throughput sequencing platform (Wide-Seq), and the data were analyzed using Bismark software. DNA methylation of PpGe in (A) ESCs and (B) F9 ECCs pre- and post-differentiation. Less than 10% DNA methylation was recorded in F9 ECCs, whereas the H19 imprinted region, used as a control, showed DNA methylation at 80%. At the same regions, DNA methylation increased up to 30% in ESCs. See also Figure S1A. (C) DNA methylation of PpGe in F9 ECCs overexpressing Myc-Dnmt3a.

(D) Gene expression analysis by qRT-PCR PpGs in F9 ECCs overexpressing Myc-Dnmt3a pre- and post-differentiation. (C) shows low levels (less than 10%) in DNA methylation at most PpGe, and (D) shows no significant decrease in expression in 5 out of 8 tested PpGs (p > 0.1). The C_t values for each gene were normalized to *Gapdh*, and expression is shown relative to that in undifferentiated cells (dotted line). (E) Genome-wide DNA methylation analysis by MethylRAD sequencing. Genomic DNA was digested with the restriction enzyme *Fsp*EI, which cuts methylated DNA into 31–32 bp fragments. The fragments were sequenced and mapped on an mm10 mouse genome. The number of reads per region were used as a measure for the extent of DNA methylation and compared between undifferentiated and D4 differentiated F9 ECCs. The waterfall plot shows DNA methylation changes at PpGe, which were computed by subtracting normalized counts in D4 samples from normalized counts in undifferentiated samples. Upper and lower quartiles were

enhancers (low-intermediate-high) were calculated based on the highest (75th percentile) and lowest (25th percentile) number of reads at all annotated enhancers in the genome, which were obtained from EnhancerAtlas 2.0. Previous studies reported that PpGe were bound by Lsd1 in ESCs, however its H3K4me1 demethylation activity was required H3K4me1 demethylation by Lsd1 the PpGe decommissioning post-differentiation, required H3K4me1 demethylation by Lsd1 (Whyte et al., 2012). In succession, our studies showed that H3K4me1 demethylation was critical for Dnmt3a-catalyzed DNA methylation at these sites (Petell et al., 2016). Therefore, we filtered the data to focus our analysis on DNA methylation changes at 3,840 PpGe previously annotated in ESCs as Lsd1-bound regions (Whyte et al., 2012). Our method identified 1,865 PpGe in F9 ECCs. Compared to methylation levels at all other known enhancers, the PpGe clustered into the low/intermediate methylation group (Figure S2B). The difference in methylation for each PpGe region was computed by subtracting the DNA methylation level in D4 differentiated from that in undifferentiated F9 ECCs. The data showed 1,488 (82%) regions failed to gain DNA methylation post-differentiation of F9 ECCs (no change in DNA methylation [NCDM]) (Figure 2E). To determine the function of genes associated with NCDM PpGe, we performed Ingenuity Pathway Analysis (IPA) (https://www.qiagen.com/ingenuity), which showed a significant enrichment of Oct4-regulated mammalian ESCs and molecular mechanisms of cancer pathways (Figure 2F).

Given that DNA methylation by Dnmt3a at PpGe requires H3K27 deacetylation and H3K4 demethylation by Lsd1/Mi2/NurD complex (Whyte et al., 2012), we anticipated that a potential impediment in this process would cause widespread failure to acquire DNA methylation at PpGe.

A "Primed" PpGe State Is Established during F9 ECC Differentiation

We asked if the chromatin state at PpGe in F9 ECCs is refractory to DNA methylation. To examine histone H3K27 deacetylation, chromatin immunoprecipitation followed by qPCR (ChIP-qPCR) was performed and showed a decrease in H3K27Ac at PpGe in F9 ECCs post-differentiation (Figure 3A). This result suggests that, similar to our observations in ESCs (Figure S3A), PpGe are active in undifferentiated F9 ECCs and initiate the decommissioning process post-differentiation. Furthermore, deacetylation at *Lefty1* and *Lefty2* enhancers suggests enhancer-switching involving the potential use of germline-specific enhancers post-differentiation, which leads to an observed

used in thresholding regions as gaining or losing methylation. The pie chart shows fractions of PpGe with increase, decrease, or no change in DNA methylation (NCDM). See also Figure S2B.

(F) Top ten statistically significant enriched canonical pathways among the genes associated with the NCDM enhancers, which showed no change. The x axis shows the log10 (adjusted p value), with the p value adjusted for multiple testing using the Benjamini-Hochberg method.

Data for (A)–(D) are the average and SEM of two biological replicates. UD, undifferentiated; D4 and D8, days post-induction of differentiation; D8 UT, untransfected F9 ECCs differentiated for 8 days; D8+Myc-Dnmt3a, F9 ECCs overexpressing Myc-Dnmt3a and differentiated for 8 days; ESCs, embryonic stem cells; F9 ECCs, F9 embryonal carcinoma cells; PpGe, pluripotency gene enhancers.
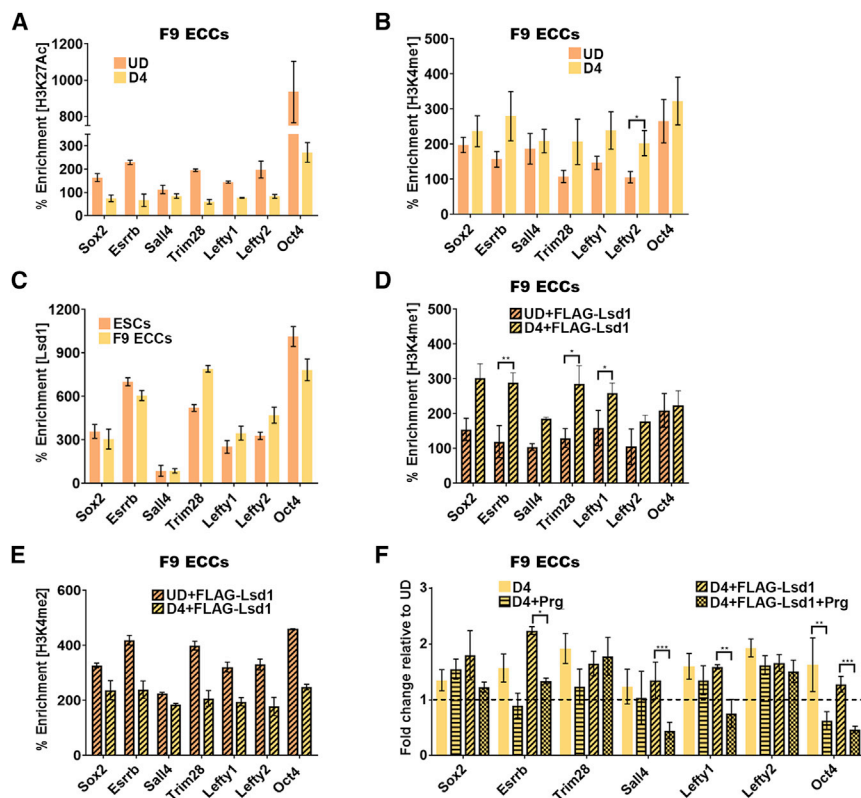
Figure 3. A "Primed" Chromatin State Is Established at Pluripotency Gene Enhancers in Embryonal Carcinoma Cells

Chromatin immunoprecipitation (ChIP)-qPCR assays.

(A and B) Histone modifications at PpGe (A) H3K27Ac and (B) H3K4me1 in F9 ECCs pre- and D4 post-differentiation. Whereas deacetylation of PpGe is observed as a decrease in the H3K27Ac signal, histone H3K4me1 is retained post-differentiation.

(C) Lsd1 occupancy in undifferentiated ESCs and F9 ECCs.

(D and E) Enrichment of (D) H3K4me1 and (E) H3K4me2 in F9 ECCs expressing recombinant FLAG-Lsd1 compared to undifferentiated transfected cells. The ECCs were differentiated 24 h post-transfection with Lsd1-expressing plasmid. Whereas there was an increase in H3K4me1 at some PpGe (D), there was a concomitant decrease in H3K4me2 enrichment (E).

(F) Fold change in enrichment of H3K4me1 at PpGe in pargyline treated and untreated, WT, and FLAG-Lsd1 overexpressing F9 ECCs at D4 post-differentiation. Fold change is represented as relative to enrichment in the undifferentiated state (dotted line).

% Enrichment = fold enrichment over input × 100. p values were derived from Student's t test: *p < 0.05; **p < 0.01; ***p < 0.005. UD, undifferentiated; D4, days post-induction of differentiation; D4+FLAG-Lsd1, F9 ECCs overexpressing FLAG-Lsd1 and differentiated for 4 days; Prg, pargyline; ESCs, embryonic stem cells; F9 ECCs, F9 embryonal carcinoma cells; PpGe, pluripotency gene enhancers. All experiments are an average of atleast two biological replicates and error is shown as SEM.

increase in *Lefty1* and *Lefty2* expression (Figure 1A). Numerous studies have proposed that deacetylation of H3K27Ac followed by H3K27 methylation by the PRC2 enzyme complex establishes a silenced state (Lindroth et al., 2008; Barski et al., 2007; Wang et al., 2008). Our data showed no increase of H3K27me3 at the PpGe in both ESCs as well as F9 ECCs post-differentiation, suggesting that PRC2 activity is nonessential for PpGe silencing (Figures S3B and S3C). H3 occupancy at the PpGe in F9 ECCs between pre- and post-differentiation was similar, supporting these conclusions (Figure S3D).

Using ChIP-qPCR, we next monitored H3K4me1 demethylation at PpGe during F9 ECC differentiation. Surprisingly, we observed a retention of H3K4me1 modification at most enhancers and a significant increase at 1 of 7 tested PpGe post-differentiation (Figure 3B), suggesting a potential disruption of Lsd1 activity. We verified similar expression levels of Lsd1 in F9 ECCs compared to ESCs (Figures S1B and S1C). Previous studies have shown Lsd1 interacts with the components of the NuRD complex in ESCs and cancer cells to facilitate deacetylation of H3K27 followed by demethylation of H3K4me1 (Whyte et al., 2012; Petell et al., 2016; Li et al., 2011b; Patel et al., 2018; Wang et al., 2009b). To examine if Lsd1 interacts with the Mi2/NuRD complex in F9 ECCs, we performed co-immunoprecipitation (coIP) experiments using whole cell extracts. We used the whole cell extract from ESCs as a positive control. Antibodies against Lsd1 and HDAC1 were used for reciprocal coIP. A strong

signal for HDAC1 and Lsd1 and a weak signal for CHD4 in both F9 ECCs and ESCs were observed (Figure S3E). An absence of signal for the acetyltransferase HBO1 in Lsd1 coIP and the presence of CHD4 support the specificity of the interaction between Lsd1 and the NuRD complex in F9 ECCs (Figure S3F). To test whether Lsd1 is recruited to PpGe, we used ChIP-qPCR, which showed a similar enrichment of Lsd1 in F9 ECCs and ESCs at PpGe (Figure 3C). These data suggest that retention of H3K4me1 at PpGe is not caused by the absence of Lsd1, but rather is due to the lack of its activity at these sites in F9 ECCs post-differentiation.

To confirm the above conclusion, we next tested the effect of overexpression or inhibition of Lsd1 on PpGe silencing and PpG repression in differentiating F9 ECCs. F9 ECCs were transfected with a FLAG-Lsd1 overexpressing plasmid and differentiated at 24 h post-transfection (Figure S4A). The recombinant Lsd1 was not able to rescue H3K4me1 demethylation at PpGe, shown by no decrease in H3K4me1 at most PpGe (Figure 3D). However, a significant increase was observed at 3 out of 7 PpGe post-differentiation. This could result from incomplete demethylation of H3K4me2 to H3K4me1 at these sites by recombinant Lsd1, confirmed by a decrease in H3K4me2 signal at most of the PpGe in Lsd1 overexpressing F9 ECCs post-differentiation (Figure 3E). These data suggest that an inhibitory mechanism affects Lsd1 demethylation activity, irrespective of its origin of expression. Additionally, Lsd1 overexpression had no significant
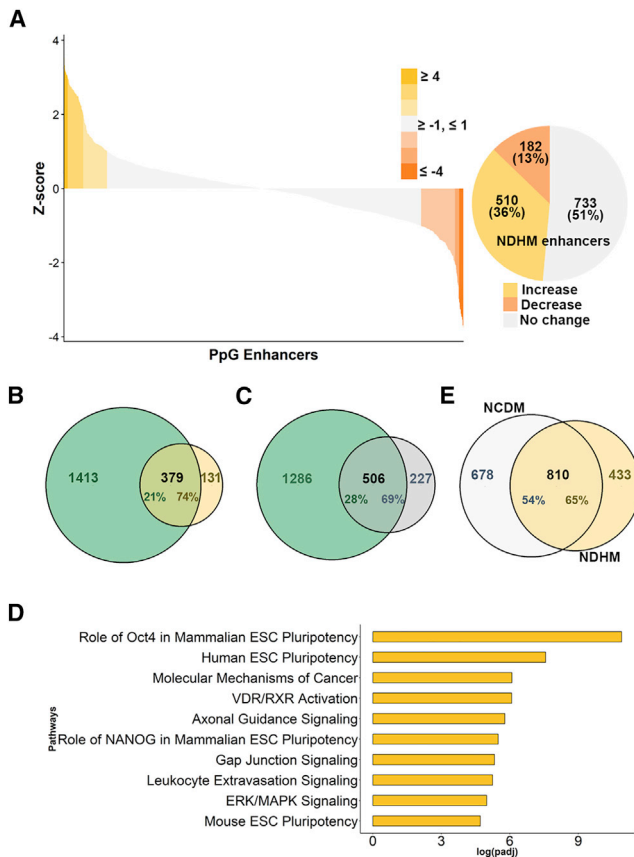
Figure 4. Global Retention of H3K4me1 at Pluripotency Gene Enhancers in Embryonal Carcinoma Cells

Genome-wide H3K4me1 levels in F9 ECCs pre- and post-differentiation were measured by ChIP-seq. Peak calling was performed using Epic2 for each input-ChIP pair. A total of 1,425 H3K4me1 peaks were identified in F9 ECCs within 1 kbp of previously annotated PpGe in ESCs (Whyte et al., 2012). See also Figure S5A. The histone demethylation activity of Lsd1 was surmised by calculating the change in H3K4me1 peak enrichment at PpGe between D4 differentiated and undifferentiated samples.

(A) Waterfall plot represents changes in H3K4me1, which were calculated as the difference between log2FC of D4 and undifferentiated samples and transformed to Z score. Z score thresholds of +1 and −1 were used to define the fractions showing increase, no change, or decrease in H3K4me1 shown in the pie chart. Taken together, 87% PpGe show an increase or no change (NDCM) in H3K4me1 enrichment.

(B and C) Venn diagrams showing an overlap between PpGe that show (B) an increase or (C) no change in peak enrichment in F9 ECCs but undergo histone H3K4me1 demethylation in ESCs post-differentiation (Whyte et al., 2012).

(D) Top ten statistically significant enriched canonical pathways among the genes associated with increase and no change in F9 ECCs. The x axis shows the log$_{10}$ (adjusted p value), with the p value adjusted for multiple testing using the Benjamini-Hochberg method.

(E) Overlap between the PpGe showing no change in DNA methylation (NDHM) and PpGe that show no decrease in H3K4me1 (NCDM).

ESCs, embryonic stem cells; F9 ECCs, F9 embryonal carcinoma cells; PpGe, pluripotency gene enhancers; D4, Days post-induction of differentiation.

effect on PpG repression or DNA methylation at PpGe post-differentiation (Figures S4B and S4C).

Previous studies in ESCs have shown that treatment with the Lsd1 inhibitor pargyline at the onset of differentiation results in

H3K4me1 retention at PpGe and incomplete repression of PpGs (Whyte et al., 2012). F9 ECCs (wild type [WT] and Lsd1 overexpressing) were treated with pargyline 6 h prior to induction of differentiation. In contrast to 70%–80% cell death caused by the Lsd1 inhibitor in ESCs, WT F9 ECCs remained largely viable upon treatment (Figure S4D), and a slight relief of repression was observed for some PpGs in these cells (Figure S4E). Whereas no decrease in H3K4me1 was observed at most PpGe in WT F9 ECCs, pargyline treatment affected the H3K4me1 enrichment at 4 out of 7 PpGe in Lsd1 overexpressing cells post-differentiation. This confirms the activity of Lsd1 at these sites, by which it converts H3K4me2 to H3K4me1 (Figure 3F). To test if Lsd1 activity contributed to the generation of H3K4me1 at PpGe in the undifferentiated state, we transiently overexpressed Lsd1 in F9 ECCs and allowed cells to grow for 72 h. ChIP-qPCR analysis showed no increase in H3K4me1 levels in Lsd1 overexpressing cells (Figure S4F). This result suggests that, similar to what has been previously reported in ESCs, the deposition of H3K4me1 in the undifferentiated F9 ECCs is largely accomplished by MLL3/4 histone methyltransferases and Lsd1 activity at these sites is initiated only in response to a differentiation signal (Wang et al., 2017, 2016; Cao et al., 2018; Whyte et al., 2012).

Taken together, these observations suggest that the restricted activity of Lsd1 at PpGe leads to retention of H3K4me1 post-differentiation. Moreover, following the deacetylation of H3K27, the absence of DNA methylation and the presence of H3K4me1 switches these enhancers to a "primed" state, prone to reactivation.

High-Throughput Analysis of Changes in H3K4me1 at PpGe

To identify all PpGe with aberrant retention of H3K4me1 post-differentiation, we performed ChIP-seq analysis of H3K4me1 genome-wide in undifferentiated and D4 differentiated F9 ECCs. Peak calling was performed using Epic2 for each input-ChIP pair, and the list was filtered to calculate the number of peaks based on defined cutoffs (false discovery rate [FDR] $\leq$ 0.05 and log2 fold change [FC] $\geq$ 2) (Figure S5A). We analyzed the distribution of H3K4me1 peaks at the regulatory elements across the genome (Figure S5B). For further analysis, we identified 1,425 H3K4me1 peaks found within 1 kilobase pair (kbp) of PpGe previously annotated in ESCs (Whyte et al., 2012). The difference in peak enrichment (i.e., log2FC) between differentiated and undifferentiated was calculated to score for changes in H3K4me1 post-differentiation. The data showed no change, increase or decrease, in 733, 510, and 182 PpGe, respectively. Therefore 87% of PpGe showed no significant decrease in H3K4me1 (no decrease in histone methylation; NDHM PpGe) (Figure 4A). We next computed the correlation between the three PpGe subgroups and the 1,792 PpGe that underwent H3K4me1 demethylation in differentiating ESCs (Whyte et al., 2012). Among the NDHM PpGe, 74% of PpGe with increased H3K4me1 and 69% PpGe with unchanged H3K4me1 in F9 ECCs overlapped with PpGe that were H3K4me1 demethylated in ESCs (Figures 4B, 4C, and S5C). These observations strongly support our previous conclusion that, in F9 ECCs, Lsd1 activity is inhibited, leading to retention of H3K4me1 at PpGe. IPA of
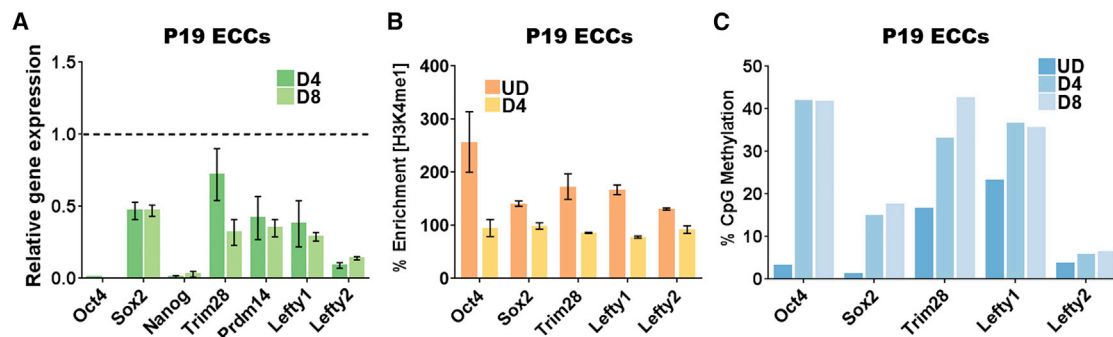
Figure 5. Pluripotency Gene Enhancers Are Decommissioned in P19 Embryonal Carcinoma Cells

(A) Gene expression analysis by qRT-PCR of PpGs in P19 ECCs. The C_t values for each gene were normalized to *Gapdh*, and expression is shown relative to that in undifferentiated cells (dotted line). Similar to the repression of PpGs in ESCs (Figure 1A), PpGs, especially Oct4 and Nanog, show more than a 90% reduction in expression.

(B) ChIP-qPCR showing H3K4me1 enrichment in UD and D4 differentiated P19 ECCs. A decrease in H3K4me1 was observed at all PpGe post-differentiation, demonstrating histone demethylation activity. % Enrichment = fold enrichment over input × 100.

(C) DNA methylation analysis of PpGe using Bis-seq in UD, D4, and D8 differentiated P19 ECCs. Up to a 40% increase in DNA methylation level was observed at 3 out of 5 PpGe post-differentiation.

All experiments are an average of at least two biological replicates and error is shown as SEM. UD, undifferentiated; D4 and D8, days post-induction of differentiation; P19 ECCs, P19 embryonal carcinoma cells; PpGs, pluripotency genes; PpGe, pluripotency gene enhancers.

NDHM PpGe-associated genes showed the highest enrichment for Oct4-regulated and stem cell pathways (Figure 4D). Comparatively, genes associated with PpGe that underwent H3K4me1 demethylation, showed enrichment for signaling pathways (Figure S5D). A correlation between NCDM and NDHM PpGe showed that 65% of the NDHM PpGe failed to acquire DNA methylation, underpinning the role of histone demethylation in the regulation of DNA methylation at PpGe (Figure 4E) (Petell et al., 2016).

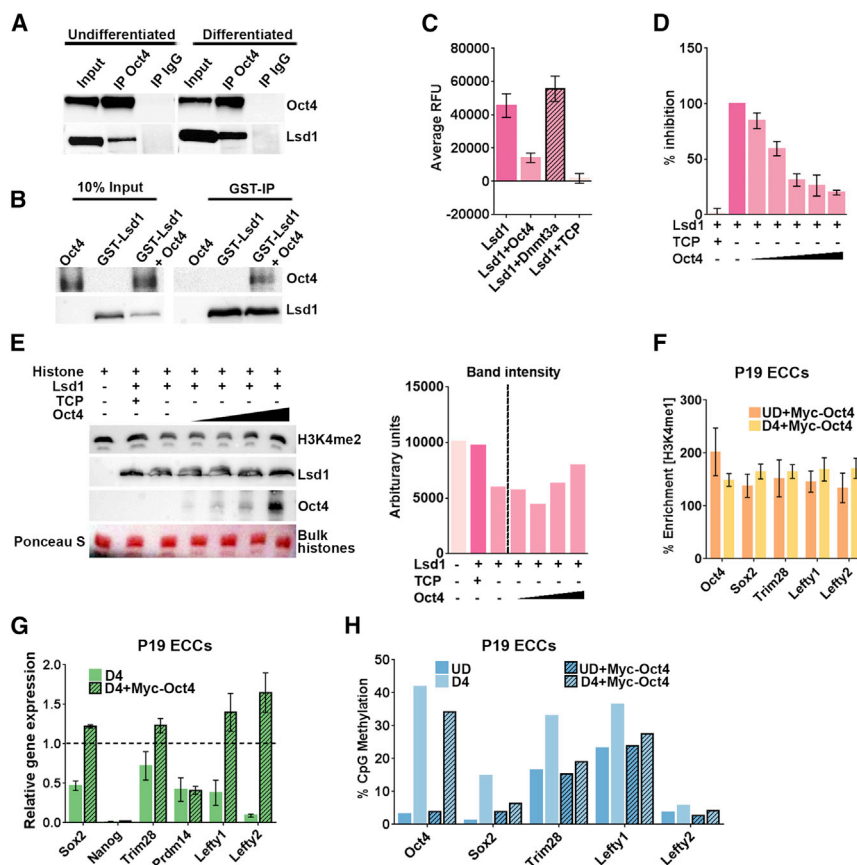**Lsd1 Activity at PpGe Is Inhibited by Its Interaction with Oct4**

Next, we sought to determine the mechanism that inhibits Lsd1 activity. Due to its continued expression in F9 ECCs post-differentiation (Figure S6A), we assumed that Oct4 remains associated with PpGe and prevents demethylation of H3K4me1 at these sites. We tested this hypothesis in P19 ECCs, in which Oct4 expression was reported to be strongly repressed post-differentiation (Li et al., 2007, 2013; Wei et al., 2007; Palmieri et al., 1994; Fuhrmann et al., 2001; Liu et al., 2011; Marikawa et al., 2011), an observation distinct from what we reported in F9 ECCs. After confirming a 90% reduction in Oct4 expression (Figure 5A), we probed H3K4me1 demethylation at PpGe during P19 ECC differentiation. Indeed, our data showed decreased enrichment of H3K4me1 at the 5 tested PpGe, D4 post-differentiation (Figure 5B). The change in chromatin state included up to a 40% gain of DNA methylation at 3 out of 5 enhancers (Figure 5C). Similar to ESCs, we also observed a massive cell death when P19 ECCs were exposed to the Lsd1 inhibitor during differentiation (Figure S6B).

Together with the pathway analysis showing enrichment of Oct4-regulated genes in NDHM and NCDM enhancers, the above data suggested that Oct4 might regulate the demethylase activity of Lsd1 at PpGe. Previous observations showing an interaction of Oct4 with Lsd1 and the Mi2/NuRD complex support this assump-tion (van den Berg et al., 2010; Pardo et al., 2010; Ding et al., 2012). The interaction of Lsd1 and Oct4 was confirmed by coIP of Lsd1 with anti-Oct4 antibody using nuclear extract from both undifferentiated and D4 differentiated F9 ECCs (Figure 6A). Co-precipitation experiments using recombinant proteins GST-Lsd1 and Oct4 revealed a direct interaction between the two proteins (Figure 6B). To test the effect of Oct4 interaction on Lsd1 catalytic activity, we performed *in vitro* Lsd1 demethylation assays using H3K4me2 peptide as a substrate. In the presence of Oct4, Lsd1 activity was reduced by 60%–70% in a dose-dependent manner. The specificity of Oct4-mediated inhibition was demonstrated by no effect of recombinant Dnmt3a protein on Lsd1 activity. Complete loss of Lsd1 activity in the presence of its inhibitor TCP (tranylcypromine) confirmed the specificity of the signal measured in this assay (Figures 6C and 6D).

We also performed Lsd1 demethylation assays using purified histones as a substrate and detected H3K4me2 demethylation on a western blot. The activity of Lsd1 was assessed by reduced H3K4me2 signal, which was rescued in the presence of 0.1 mM TCP. An accumulation of H3K4me2 signal with an increase in Oct4 concentration in the reaction mix clearly showed increased inhibition of Lsd1 activity by Oct4 (Figure 6E). These data suggest that Oct4 could inhibit Lsd1 activity at PpGe in ECCs post-differentiation. We tested this by stably expressing recombinant Oct4 in P19 ECCs (Figure S6C). Upon differentiation, the retention of H3K4me1 at PpGe indicates the inhibition of Lsd1 by the recombinant Oct4 (Figure 6F). Moreover, several PpGs were incompletely repressed with reduced gain in DNA methylation at their respective enhancers (Figures 6G and 6H). These data suggest that, in F9 ECCs, due to its continued expression post-differentiation, Oct4 remains bound at PpGe and inhibits Lsd1 activity.

Taken together, we propose the following model to explain the regulation of Lsd1 activity at PpGe. At the active PpGe, Lsd1 is inhibited by its interaction with bound Oct4.
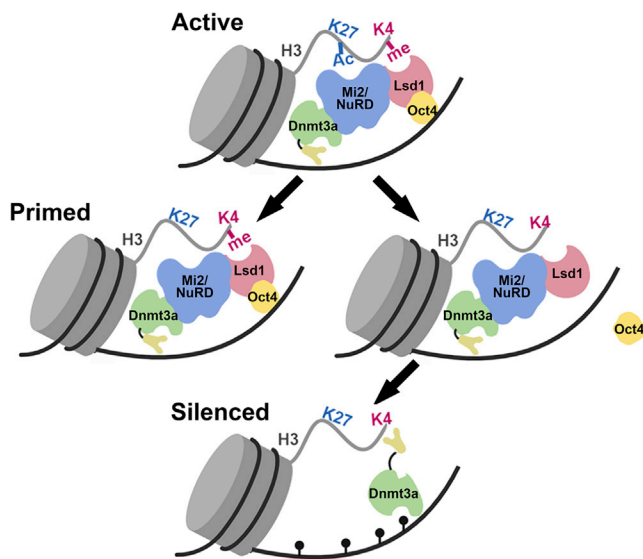
Figure 6. Oct4 Interacts with Lsd1 and Inhibits Its Catalytic Activity

(A) Nuclear extract from undifferentiated and D4 differentiated F9 ECCs was used to perform coIP with anti-Oct4 antibody and control immunoglobulin G (IgG). 10% of the input and eluate from coIP were probed for Oct4 and Lsd1 on western blot. The vertical space denotes the extra lane in the gel that was digitally removed.

(B) Glutathione S-transferase (GST) pull-down experiment showing direct interaction between Lsd1 and Oct4. Recombinant GST-Lsd1 was incubated with Oct4 at about a 1:2 molar ratio and precipitated using GST-Sepharose. The co-precipitated Oct4 is detected using anti-Oct4 antibody. The vertical space denotes the extra lane in the gel that was digitally removed.

(C) Lsd1 demethylase assay was performed using 0.25 μM Lsd1 and H3K4me2 peptide as substrate. Lsd1 demethylation activity was completely inhibited by 0.1 mM TCP (tranylcypromine) in the reaction. To test the effect of Oct4 on Lsd1 activity, demethylation assays were performed in the presence of 0.5 μM Oct4 at a 1:2 (Lsd1:Oct4) molar ratio. The catalytic domain of Dnmt3a at the same molar ratio was used as a control.

(D) Dose-dependent inhibition assays were performed using increasing concentrations of Oct4 in the following molar ratios of Lsd1:Oct4: (1:0.5), (1:1), (1:2), (1:3), (1:4). Data are an average and SD of at least 5 experimental replicates.

(E) Lsd1 demethylation assays were performed using 0.25 μM Lsd1 and 30 μg bulk histones as substrate with increasing concentrations of Oct4 in the reaction. Upper panel: histone demethylation was detected by using anti-H3K4me2 on a western blot, which shows retention of signal with increasing concentrations of Oct4. Lower panels: amount of Lsd1 enzyme and increasing amounts of Oct4 in the histone demethylation reaction. Ponceau S stain of bulk histones shows equal loading on the gel. The bar graph on the right shows quantification of H3K4me2 signal using ImageJ software.

(F) ChIP-qPCR showing percent enrichment of H3K4me1 at PpGe in P19 ECCs stably expressing recombinant Myc-Oct4 pre- and post-differentiation. The data show retention of H3K4me1 post-differentiation. % Enrichment = fold enrichment over input × 100

(G) Gene expression analysis by qRT-PCR of PpGs in P19 ECCs expressing recombinant Myc-Oct4. The C_t values were normalized to *Gapdh*, and expression is shown relative to that in undifferentiated cells (dotted line).

(H) DNA methylation analysis of PpGe using Bis-seq in UD and D4 differentiated P19 ECCs WT and expressing recombinant Myc-Oct4. Oct4 expressing cells show failure to gain DNA methylation at PpGe post-differentiation compared to untransfected WT.

All experiments are an average of at least two biological replicates and error is shown as SEM. TCP, tranylcypromine; ECCs, embryonal carcinoma cells; PpGe, pluripotency gene enhancers; D4, days post-induction of differentiation.

Post-differentiation, this inhibition is relieved by dissociation of Oct4 from its binding sites. However, in cancer cells where Oct4 expression is maintained, Lsd1 is held in its inhibited state, leading to incomplete histone demethylation. Retention of H3K4me1, in turn, blocks the activation of Dnmt3a from its auto-inhibited state, resulting in an absence of DNA methylation at PpGe (Petell et al., 2016; Guo et al., 2015; Li et al., 2011a; Ooi et al., 2007; Otani et al., 2009). The absence of DNA methylation and the presence of H3K4me1 switch these enhancers to a "primed" state, prone to activation in the presence of the coactivator (Figure 7). Based on previous reports that Oct4 as well as Lsd1 are aberrantly expressed in several cancers (Kim et al., 2015; Wang et al., 2010, 2009b; Schoenhals et al., 2009; Kashyap et al., 2013; Lv et al., 2012; Hosseini and Minucci, 2017), we suspect that Oct4-Lsd1 interaction at Oct4-bound regions will disrupt Lsd1 activity, leading to aberrant gene expression.

DISCUSSION

The epigenetic state of enhancers is preserved in various cell types, suggesting that aberrant changes could promote tumorigenesis. This phenomenon is supported by recent studies revealing a crucial role for enhancer-mediated activation of oncogenes (Hnisz et al., 2015; Mansour et al., 2014; Chapuy et al., 2013; Gröschel et al., 2014; Lovén et al., 2013). Changes in H3K4me1 levels and DNA accessibility at various enhancers have been reported in many cancers (Akhtar-Zaidi et al., 2012). Some studies also propose that changes in enhancer states play a role in the development of therapy-resistant cancer cells. These studies showed loss or gain of H3K4me1/2 at the enhancers in resistant breast cancer cells and loss of H3K27 acetylation at enhancers in T cell acute lymphoblastic leukemia (T-ALL) (Magnani et al., 2013; Knoechel et al., 2014). In addition,

Figure 7. Model of Epigenetic Changes at Pluripotency Gene Enhancers during Stem Cell Differentiation

In an undifferentiated state, the pluripotency gene enhancers (PpGe) are active, bound by the coactivator complex, and contain chromatin modifications, including H3K4m2/1 and H3K27Ac. In response to the signal of differentiation, the dissociation of the coactivator complex, including Oct4, is followed by the activity of the Lsd1-Mi2/NuRD complex, which facilitates enhancer silencing. The histone deacetylase (HDAC) removes H3K27Ac at PpGe, and Lsd1 demethylates H3K4me1, followed by DNA methylation by Dnmt3a. However, in F9 ECCs, Lsd1 activity is inhibited in the presence of Oct4, causing retention of H3K4me1. The ADD domain of Dnmt3a cannot interact with the H3K4 methylated histone tail and will potentially remain in the autoinhibited state, thus preventing DNA methylation at these sites. Consequently, PpGe, instead of being silenced, acquire a "primed" state. Black pins represent methylated CpGs.

DNA hypermethylation, concomitant with overexpression of DNA methyltransferases, is a hallmark of many cancers (Jones et al., 2016; Schübeler, 2015). Changes in DNA methylation at enhancers occur in breast, lung, prostate, and cervical cancers (Taberlay et al., 2014; Aran and Hellman, 2013; Aran et al., 2013; Yegnasubramanian et al., 2011). These studies suggest that the chromatin state of tissue-specific enhancers can be used as a diagnostic to predict aberrant expression of their respective genes in cancer. This prediction is supported by our data here and previous studies, which show that PpGe gain DNA methylation and lose H3K4me1 in differentiating ESCs, whereas, in ECCs, the absence of DNA methylation is accompanied by retention of H3K4me1 at these sites. The tissue specificity of the enhancer state is further highlighted by our data, which show that, during ESC differentiation, all tested PpGe undergo repressive chromatin changes irrespective of the transcriptional status of the associated gene. This observation is exemplified by H3K27Ac deacetylation and gain of DNA methylation at *Sox2* and *Trim28* enhancers despite the maintained expression of these genes.

Histone demethylase, Lsd1, catalyzes demethylation of dimethyl (me2) and monomethyl (me1) at K4 of histone H3 (Shi et al., 2004). The catalytic activity of Lsd1 was shown to be regulated by post-translational modification, alternative splicing, and interaction with several factors (Carnesecchi et al., 2017; Laurent et al., 2015; Metzger et al., 2005; Shi et al., 2005; Speranzini et al., 2017; Wang et al., 2015a; Zibetti et al., 2010; McClellan et al., 2019; Vinyard et al., 2019). Genetic knockout of the histone demethylase, Lsd1, was also shown to cause genome-wide loss of DNA methylation in late passage ESCs due to degradation of the DNMT1 enzyme (Wang et al., 2009a). Our previous studies demonstrated the critical role of H3K4me1 demethylation by Lsd1 in guiding DNMT3A-mediated DNA methylation at PpGe, causing enhancer silencing in ESCs (Petell et al., 2016). In contrary to ESCs, our data in differentiating F9 ECCs shows that PpGs are partially repressed and their respective enhancers retain H3K4me1 and DNA hypomethylation. The transgenic overexpression of Dnmt3A or Lsd1 in F9 ECCs was unable to rescue H3K4me1 demethylation and gain of DNA methylation at these PpGe. A small gain of DNA methylation (15%) was observed at the Oct4 enhancers in Dnmt3A-overexpressing cells; however, this was insufficient to further downregulate the expression of Oct4. This could be explained by retention of histone H3K4me1 that prevents Oct4 enhancer from silencing. Moreover, we show that complete repression of Oct4 gene during P19 ECC differentiation is accompanied by gain of 40% DNA methylation and H3K4me1 demethylation Figure 5. These data are in agreement with previous studies showing a similar accumulation of DNA methylation at the Oct4 enhancer (40%–50%) when the Oct4 gene is repressed in ESC post-differentiation (Athanasiadou et al., 2010; Petell et al., 2016). This suggests that higher DNA methylation levels are required for complete silencing of the Oct4 enhancer. Taken together, we conclude that compromised activity of Lsd1 results in the retention of H3K4me1 and the absence of DNA methylation at the PpGe, leading to a primed state of enhancers in cancer cells. Thus, our data reveal a mechanism by which developmental enhancers could acquire aberrant histone modification and DNA methylation states that affect gene expression. Unlike the silenced state, the "primed" enhancer state is accesible to coactivator binding, which renders cells vulnerable to a small increase in the expression of oncogenic coactivators or master transcription factors (Zaret and Carroll, 2011; Calo and Wysocka, 2013).

Our studies highlight the versatile regulation of Lsd1 activity, which can be fine-tuned by its interaction with numerous factors, allowing the enzyme to function in various cellular processes, during differentiation and in disease. Here we discovered that Lsd1 activity is inhibited by its interaction with the pioneer transcription factor Oct4, which is expressed at a substantial level in F9 ECCs post-differentiation. Persistent *Oct4* expression in F9 ECCs post differentiation, compared to ESCs, was also reported from flow cytometric analysis (Gordeeva and Khaydukov, 2017). Notably, aberrant expression of *Oct4*, *Sox2*, and *Nanog* is associated with tumor transformation, metastasis, and drug resistance (Sampieri and Fodde, 2012; Ben-Porath et al., 2008). We speculate that, during differentiation of CSCs, inhibition of Lsd1 by Oct4 leads to PpGe priming and/or reactivation and an enhanced PpG expression. Hence, these observations provide an insight into mechanism mediating the reistance of cancer stem cells to differentiation therapy and may promote novel approaches to improve it.

STAR★METHODS

Detailed methods are provided in the online version of this paper and include the following:

- KEY RESOURCES TABLE
- LEAD CONTACT AND MATERIALS AVAILABILITY
- EXPERIMENTAL MODEL AND SUBJECT DETAILS
- METHOD DETAILS
  - DNA methylation analysis
  - Chromatin Immunoprecipitation and ChIP-Seq
  - Gene expression analysis
  - Microscopy
  - Co-precipitation assays
  - *In vitro* Lsd1 demethylase activity assay
  - Histone demethylation assay
  - Co-immunoprecipitation
  - Western blot
  - MethylRAD sequencing Analysis
  - ChIP-Seq Analysis
  - Pathway Analysis
- QUANTIFICATION AND STATISTICAL ANALYSIS
  - methylRAD statistical analyses and software
  - ChIP-seq statistical analyses and software
  - Pathway analyses
- DATA AND CODE AVAILABILITY

SUPPLEMENTAL INFORMATION

Supplemental Information can be found online at https://doi.org/10.1016/j.celrep.2019.11.040.

AUTHORS CONTRIBUTIONS

L.A., S.M., B.H., J.B., M.H., D.S., and M.S.D. performed the experiments. N.A., S.U., and P.A.S. analyzed the genome-wide data. L.A. and H.G. wrote the manuscript.

DECLARATION OF INTERESTS

The authors declare no competing interests.

REFERENCES

Akhtar-Zaidi, B., Cowper-Sal-lari, R., Corradin, O., Saiakhova, A., Bartels, C.F., Balasubramanian, D., Myeroff, L., Lutterbaugh, J., Jarrar, A., Kalady, M.F., et al. (2012). Epigenomic enhancer profiling defines a signature of colon cancer. Science *336*, 736–739.

Alonso, A., Breuer, B., Steuer, B., and Fischer, J. (1991). The F9-EC cell line as a model for the analysis of differentiation. Int. J. Dev. Biol. *35*, 389–397.

Andrews, S. (2010). FastQC: a quality control tool for high throughput sequence data. http://www.bioinformatics.babraham.ac.uk/projects/fastqc.

Andrews, P.W., Matin, M.M., Bahrami, A.R., Damjanov, I., Gokhale, P., and Draper, J.S. (2005). Embryonic stem (ES) cells and embryonal carcinoma (EC) cells: opposite sides of the same coin. Biochem. Soc. Trans. *33*, 1526–1530.

Aran, D., and Hellman, A. (2013). DNA methylation of transcriptional enhancers and cancer predisposition. Cell *154*, 11–13.

Aran, D., Sabato, S., and Hellman, A. (2013). DNA methylation of distal regulatory sites characterizes dysregulation of cancer genes. Genome Biol. *14*, R21.

Athanasiadou, R., de Sousa, D., Myant, K., Merusi, C., Stancheva, I., and Bird, A. (2010). Targeting of de novo DNA methylation throughout the Oct-4 gene regulatory region in differentiating embryonic stem cells. PLoS ONE *5*, e9937.

Banerji, J., Rusconi, S., and Schaffner, W. (1981). Expression of a beta-globin gene is enhanced by remote SV40 DNA sequences. Cell *27*, 299–308.

Baron, R., Binda, C., Tortorici, M., McCammon, J.A., and Mattevi, A. (2011). Molecular mimicry and ligand recognition in binding and catalysis by the histone demethylase LSD1-CoREST complex. Structure *19*, 212–220.

Barski, A., Cuddapah, S., Cui, K., Roh, T.-Y., Schones, D.E., Wang, Z., Wei, G., Chepelev, I., and Zhao, K. (2007). High-resolution profiling of histone methylations in the human genome. Cell *129*, 823–837.

Ben-Porath, I., Thomson, M.W., Carey, V.J., Ge, R., Bell, G.W., Regev, A., and Weinberg, R.A. (2008). An embryonic stem cell-like gene expression signature in poorly differentiated aggressive human tumors. Nat. Genet. *40*, 499–507.

Bolger, A.M., Lohse, M., and Usadel, B. (2014). Trimmomatic: a flexible trimmer for Illumina sequence data. Bioinformatics *30*, 2114–2120.

Bulger, M., and Groudine, M. (2011). Functional and mechanistic diversity of distal transcription enhancers. Cell *144*, 327–339.

Calo, E., and Wysocka, J. (2013). Modification of enhancer chromatin: what, how, and why? Mol. Cell *49*, 825–837.

Cao, K., Collings, C.K., Morgan, M.A., Marshall, S.A., Rendleman, E.J., Ozark, P.A., Smith, E.R., and Shilatifard, A. (2018). An Mll4/COMPASS-Lsd1 epigenetic axis governs enhancer function and pluripotency transition in embryonic stem cells. Sci Adv. *4*, eaap8747.

Carnesecchi, J., Forcet, C., Zhang, L., Tribollet, V., Barenton, B., Boudra, R., Cerutti, C., Billas, I.M., Sérandour, A.A., Carroll, J.S., et al. (2017). ERRα induces H3K9 demethylation by LSD1 to promote cell invasion. Proc. Natl. Acad. Sci. USA *114*, 3909–3914.

Chapuy, B., McKeown, M.R., Lin, C.Y., Monti, S., Roemer, M.G., Qi, J., Rahl, P.B., Sun, H.H., Yeda, K.T., Doench, J.G., et al. (2013). Discovery and characterization of super-enhancer-associated dependencies in diffuse large B cell lymphoma. Cancer Cell *24*, 777–790.

Cohen-Karni, D., Xu, D., Apone, L., Fomenkov, A., Sun, Z., Davis, P.J., Kinney, S.R., Yamada-Mabuchi, M., Xu, S.Y., Davis, T., et al. (2011). The MspJI family of modification-dependent restriction endonucleases for epigenetic studies. Proc. Natl. Acad. Sci. USA *108*, 11040–11045.

Creyghton, M.P., Cheng, A.W., Welstead, G.G., Kooistra, T., Carey, B.W., Steine, E.J., Hanna, J., Lodato, M.A., Frampton, G.M., Sharp, P.A., et al. (2010). Histone H3K27ac separates active from poised enhancers and predicts developmental state. Proc. Natl. Acad. Sci. USA *107*, 21931–21936.

de Thé, H. (2018). Differentiation therapy revisited. Nat. Rev. Cancer *18*, 117–127.

Ding, J., Xu, H., Faiola, F., Ma'ayan, A., and Wang, J. (2012). Oct4 links multiple epigenetic pathways to the pluripotency network. Cell Res. *22*, 155–167.

Ernst, J., and Kellis, M. (2010). Discovery and characterization of chromatin states for systematic annotation of the human genome. Nat. Biotechnol. *28*, 817–825.

Ernst, J., Kheradpour, P., Mikkelsen, T.S., Shoresh, N., Ward, L.D., Epstein, C.B., Zhang, X., Wang, L., Issner, R., Coyne, M., et al. (2011). Mapping and analysis of chromatin state dynamics in nine human cell types. Nature 473, 43–49.

Feske, S. (2007). Calcium signalling in lymphocyte activation and disease. Nat. Rev. Immunol. 7, 690–702.

Fuhrmann, G., Chung, A.C., Jackson, K.J., Hummelke, G., Baniahmad, A., Sutter, J., Sylvester, I., Schöler, H.R., and Cooney, A.J. (2001). Mouse germline restriction of Oct4 expression by germ cell nuclear factor. Dev. Cell 1, 377–387.

Gao, T., and Qian, J. (2019). EnhancerAtlas 2.0: an updated resource with enhancer annotation in 586 tissue/cell types across nine species. Nucleic Acids Res. Published online November 19, 2019. https://doi.org/10.1093/nar/gkz980.

Gao, X.N., Yan, F., Lin, J., Gao, L., Lu, X.L., Wei, S.C., Shen, N., Pang, J.X., Ning, Q.Y., Komeno, Y., et al. (2015). AML1/ETO cooperates with HIF1α to promote leukemogenesis through DNMT3a transactivation. Leukemia 29, 1730–1740.

Gao, T., He, B., Liu, S., Zhu, H., Tan, K., and Qian, J. (2016). EnhancerAtlas: a resource for enhancer annotation and analysis in 105 human cell/tissue types. Bioinformatics 32, 3543–3551.

Gordeeva, O., and Khaydukov, S. (2017). Tumorigenic and Differentiation Potentials of Embryonic Stem Cells Depend on TGFβ Family Signaling: Lessons from Teratocarcinoma Cells Stimulated to Differentiate with Retinoic Acid. Stem Cells Int. 2017, 7284872.

Gröschel, S., Sanders, M.A., Hoogenboezem, R., de Wit, E., Bouwman, B.A.M., Erpelinck, C., van der Velden, V.H.J., Havermans, M., Avellino, R., van Lom, K., et al. (2014). A single oncogenic enhancer rearrangement causes concomitant EVI1 and GATA2 deregulation in leukemia. Cell 157, 369–381.

Guo, X., Wang, L., Li, J., Ding, Z., Xiao, J., Yin, X., He, S., Shi, P., Dong, L., Li, G., et al. (2015). Structural insight into autoinhibition and histone H3-induced activation of DNMT3A. Nature 517, 640–644.

Gwak, J.M., Kim, M., Kim, H.J., Jang, M.H., and Park, S.Y. (2017). Expression of embryonal stem cell transcription factors in breast cancer: Oct4 as an indicator for poor clinical outcome and tamoxifen resistance. Oncotarget 8, 36305–36318.

Han, J.W., Gurunathan, S., Choi, Y.J., and Kim, J.H. (2017). Dual functions of silver nanoparticles in F9 teratocarcinoma stem cells, a suitable model for evaluating cytotoxicity- and differentiation-mediated cancer therapy. Int. J. Nanomedicine 12, 7529–7549.

Heintzman, N.D., Stuart, R.K., Hon, G., Fu, Y., Ching, C.W., Hawkins, R.D., Barrera, L.O., Van Calcar, S., Qu, C., Ching, K.A., et al. (2007). Distinct and predictive chromatin signatures of transcriptional promoters and enhancers in the human genome. Nat. Genet. 39, 311–318.

Heinz, S., Benner, C., Spann, N., Bertolino, E., Lin, Y.C., Laslo, P., Cheng, J.X., Murre, C., Singh, H., and Glass, C.K. (2010). Simple combinations of lineage-determining transcription factors prime cis-regulatory elements required for macrophage and B cell identities. Mol. Cell 38, 576–589.

Heinz, S., Romanoski, C.E., Benner, C., and Glass, C.K. (2015). The selection and function of cell type-specific enhancers. Nat. Rev. Mol. Cell Biol. 16, 144–154.

Hnisz, D., Schuijers, J., Lin, C.Y., Weintraub, A.S., Abraham, B.J., Lee, T.I., Bradner, J.E., and Young, R.A. (2015). Convergence of developmental and oncogenic signaling pathways at transcriptional super-enhancers. Mol. Cell 58, 362–370.

Hosseini, A., and Minucci, S. (2017). A comprehensive review of lysine-specific demethylase 1 and its roles in cancer. Epigenomics 9, 1123–1142.

Iglesias, J.M., Gumuzio, J., and Martin, A.G. (2017). Linking Pluripotency Reprogramming and Cancer. Stem Cells Transl. Med. 6, 335–339.

Jeter, C.R., Liu, B., Liu, X., Chen, X., Liu, C., Calhoun-Davis, T., Repass, J., Zaehres, H., Shen, J.J., and Tang, D.G. (2011). NANOG promotes cancer stem cell characteristics and prostate cancer resistance to androgen deprivation. Oncogene 30, 3833–3845.

Jones, P.A., Issa, J.-P.J., and Baylin, S. (2016). Targeting the cancer epigenome for therapy. Nat. Rev. Genet. 17, 630–641.

Kashyap, V., Ahmad, S., Nilsson, E.M., Helczynski, L., Kenna, S., Persson, J.L., Gudas, L.J., and Mongan, N.P. (2013). The lysine specific demethylase-1 (LSD1/KDM1A) regulates VEGF-A expression in prostate cancer. Mol. Oncol. 7, 555–566.

Kim, B.W., Cho, H., Choi, C.H., Ylaya, K., Chung, J.Y., Kim, J.H., and Hewitt, S.M. (2015). Clinical significance of OCT4 and SOX2 protein expression in cervical cancer. BMC Cancer 15, 1015.

Knoechel, B., Roderick, J.E., Williamson, K.E., Zhu, J., Lohr, J.G., Cotton, M.J., Gillespie, S.M., Fernandez, D., Ku, M., Wang, H., et al. (2014). An epigenetic mechanism of resistance to targeted therapy in T cell acute lymphoblastic leukemia. Nat. Genet. 46, 364–370.

Krueger, F., and Andrews, S.R. (2011). Bismark: a flexible aligner and methylation caller for Bisulfite-Seq applications. Bioinformatics. 27, 1571–1572.

Krueger, F. (2012). Trim Galore: A wrapper tool around Cutadapt and FastQC to consistently apply quality and adapter trimming to FastQ files. http://www.bioinformatics.babraham.ac.uk/projects/trim_galore/.

Kumar, S.M., Liu, S., Lu, H., Zhang, H., Zhang, P.J., Gimotty, P.A., Guerra, M., Guo, W., and Xu, X. (2012). Acquired cancer stem cell phenotypes through Oct4-mediated dedifferentiation. Oncogene 31, 4898–4911.

Langmead, B., and Salzberg, S.L. (2012). Fast gapped-read alignment with Bowtie 2. Nat. Methods 9, 357–359.

Langmead, B., Trapnell, C., Pop, M., and Salzberg, S.L. (2009). Ultrafast and memory-efficient alignment of short DNA sequences to the human genome. Genome Biol. 10, R25.

Laurent, B., Ruitu, L., Murn, J., Hempel, K., Ferrao, R., Xiang, Y., Liu, S., Garcia, B.A., Wu, H., Wu, F., et al. (2015). A specific LSD1/KDM1A isoform regulates neuronal differentiation through H3K9 demethylation. Mol. Cell 57, 957–970.

Li, J.Y., Pu, M.T., Hirasawa, R., Li, B.Z., Huang, Y.N., Zeng, R., Jing, N.H., Chen, T., Li, E., Sasaki, H., and Xu, G.L. (2007). Synergistic function of DNA methyltransferases Dnmt3a and Dnmt3b in the methylation of Oct4 and Nanog. Mol. Cell. Biol. 27, 8748–8759.

Li, B.Z., Huang, Z., Cui, Q.Y., Song, X.H., Du, L., Jeltsch, A., Chen, P., Li, G., Li, E., and Xu, G.L. (2011a). Histone tails regulate DNA methylation by allosterically activating de novo methyltransferase. Cell Res. 21, 1172–1181.

Li, Q., Shi, L., Gui, B., Yu, W., Wang, J., Zhang, D., Han, X., Yao, Z., and Shang, Y. (2011b). Binding of the JmjC demethylase JARID1B to LSD1/NuRD suppresses angiogenesis and metastasis in breast cancer cells by repressing chemokine CCL14. Cancer Res. 71, 6899–6908.

Li, H., Fan, R., Sun, M., Jiang, T., and Gong, Y. (2013). Nspc1 regulates the key pluripotent Oct4-Nanog-Sox2 axis in P19 embryonal carcinoma cells via directly activating Oct4. Biochem. Biophys. Res. Commun. 440, 527–532.

Lindroth, A.M., Park, Y.J., McLean, C.M., Dokshin, G.A., Persson, J.M., Herman, H., Pasini, D., Miró, X., Donohoe, M.E., Lee, J.T., et al. (2008). Antagonism between DNA and H3K27 methylation at the imprinted Rasgrf1 locus. PLoS Genet. 4, e1000145.

Linn, D.E., Yang, X., Sun, F., Xie, Y., Chen, H., Jiang, R., Chen, H., Chumsri, S., Burger, A.M., and Qiu, Y. (2010). A Role for OCT4 in Tumor Initiation of Drug-Resistant Prostate Cancer Cells. Genes Cancer 1, 908–916.

Liu, H., Deng, S., Zhao, Z., Zhang, H., Xiao, J., Song, W., Gao, F., and Guan, Y. (2011). Oct4 regulates the miR-302 cluster in P19 mouse embryonic carcinoma cells. Mol. Biol. Rep. 38, 2155–2160.

Liu, A., Yu, X., and Liu, S. (2013). Pluripotency transcription factors and cancer stem cells: small genes make a big difference. Chin. J. Cancer 32, 483–487.

Lovén, J., Hoke, H.A., Lin, C.Y., Lau, A., Orlando, D.A., Vakoc, C.R., Bradner, J.E., Lee, T.I., and Young, R.A. (2013). Selective inhibition of tumor oncogenes by disruption of super-enhancers. Cell 153, 320–334.

Lv, T., Yuan, D., Miao, X., Lv, Y., Zhan, P., Shen, X., and Song, Y. (2012). Overexpression of LSD1 promotes proliferation, migration and invasion in non-small cell lung cancer. PLoS ONE 7, e35065.

Lyko, F. (2018). The DNA methyltransferase family: a versatile toolkit for epigenetic regulation. Nat. Rev. Genet. *19*, 81–92.

Ma, H.S., Wang, E.L., Xu, W.F., Yamada, S., Yoshimoto, K., Qian, Z.R., Shi, L., Liu, L.L., and Li, X.H. (2018). Overexpression of DNA (Cytosine-5)-Methyltransferase 1 (DNMT1) And DNA (Cytosine-5)-Methyltransferase 3A (DNMT3A) Is Associated with Aggressive Behavior and Hypermethylation of Tumor Suppressor Genes in Human Pituitary Adenomas. Med. Sci. Monit. *24*, 4841–4850.

Magnani, L., Stoeck, A., Zhang, X., Lánczky, A., Mirabella, A.C., Wang, T.-L., Gyorffy, B., and Lupien, M. (2013). Genome-wide reprogramming of the chromatin landscape underlies endocrine therapy resistance in breast cancer. Proc Natl Acad Sci U S A. *110*, E1490–E1499.

Mak, V.C., Siu, M.K., Wong, O.G., Chan, K.K., Ngan, H.Y., and Cheung, A.N. (2012). Dysregulated stemness-related genes in gynecological malignancies. Histol. Histopathol. *27*, 1121–1130.

Mansour, M.R., Abraham, B.J., Anders, L., Berezovskaya, A., Gutierrez, A., Durbin, A.D., Etchin, J., Lawton, L., Sallan, S.E., Silverman, L.B., et al. (2014). Oncogene regulation. An oncogenic super-enhancer formed through somatic mutation of a noncoding intergenic element. Science *346*, 1373–1377.

Marikawa, Y., Tamashiro, D.A., Fujita, T.C., and Alarcon, V.B. (2011). Dual roles of Oct4 in the maintenance of mouse P19 embryonal carcinoma cells: as negative regulator of Wnt/β-catenin signaling and competence provider for Brachyury induction. Stem Cells Dev. *20*, 621–633.

Martin, M. (2011). Cutadapt removes adapter sequences from high-throughput sequencing reads. EMBnet.journal *17*, 10–12.

McClellan, D., Casey, M.J., Bareyan, D., Lucente, H., Ours, C., Velinder, M., Singer, J., Lone, M.D., Sun, W., Coria, Y., Mason, C., and Engel, M.E. (2019). Growth Factor Independence (GFI) 1B-mediated transcriptional repression and lineage allocation require Lysine Specific Demethylase (LSD)1-dependent recruitment of the BHC complex. Mol Cell Biol. *39*, pii: e00020-19.

Mendenhall, E.M., Williamson, K.E., Reyon, D., Zou, J.Y., Ram, O., Joung, J.K., and Bernstein, B.E. (2013). Locus-specific editing of histone modifications at endogenous enhancers. Nat. Biotechnol. *31*, 1133–1136.

Metzger, E., Wissmann, M., Yin, N., Müller, J.M., Schneider, R., Peters, A.H., Günther, T., Buettner, R., and Schüle, R. (2005). LSD1 demethylates repressive histone marks to promote androgen-receptor-dependent transcription. Nature *437*, 436–439.

Ong, C.-T., and Corces, V.G. (2011). Enhancer function: new insights into the regulation of tissue-specific gene expression. Nat. Rev. Genet. *12*, 283–293.

Ooi, S.K., Qiu, C., Bernstein, E., Li, K., Jia, D., Yang, Z., Erdjument-Bromage, H., Tempst, P., Lin, S.P., Allis, C.D., et al. (2007). DNMT3L connects unmethylated lysine 4 of histone H3 to de novo methylation of DNA. Nature *448*, 714–717.

Otani, J., Nankumo, T., Arita, K., Inamoto, S., Ariyoshi, M., and Shirakawa, M. (2009). Structural basis for recognition of H3K4 methylation status by the DNA methyltransferase 3A ATRX-DNMT3-DNMT3L domain. EMBO Rep. *10*, 1235–1241.

Palmieri, S.L., Peter, W., Hess, H., and Schöler, H.R. (1994). Oct-4 transcription factor is differentially expressed in the mouse embryo during establishment of the first two extraembryonic cell lineages involved in implantation. Dev. Biol. *166*, 259–267.

Pardo, M., Lang, B., Yu, L., Prosser, H., Bradley, A., Babu, M.M., and Choudhary, J. (2010). An expanded Oct4 interaction network: implications for stem cell biology, development, and disease. Cell Stem Cell *6*, 382–395.

Patel, D., Shimomura, A., Majumdar, S., Holley, M.C., and Hashino, E. (2018). The histone demethylase LSD1 regulates inner ear progenitor differentiation through interactions with Pax2 and the NuRD repressor complex. PLoS ONE *13*, e0191689.

Peng, S., Maihle, N.J., and Huang, Y. (2010). Pluripotency factors Lin28 and Oct4 identify a sub-population of stem cell-like cells in ovarian cancer. Oncogene *29*, 2153–2159.

Petell, C.J., Alabdi, L., He, M., San Miguel, P., Rose, R., and Gowher, H. (2016). An epigenetic switch regulates de novo DNA methylation at a subset of pluripotency gene enhancers during embryonic stem cell differentiation. Nucleic Acids Res. *44*, 7605–7617.

Plank, J.L., and Dean, A. (2014). Enhancer function: mechanistic and genome-wide insights come together. Mol. Cell *55*, 5–14.

Quinlan, A.R., and Hall, I.M. (2010). BEDTools: a flexible suite of utilities for comparing genomic features. Bioinformatics. *26*, 841–842.

Rada-Iglesias, A., Bajpai, R., Swigut, T., Brugmann, S.A., Flynn, R.A., and Wysocka, J. (2011). A unique chromatin signature uncovers early developmental enhancers in humans. Nature *470*, 279–283.

Sampieri, K., and Fodde, R. (2012). Cancer stem cells and metastasis. Semin. Cancer Biol. *22*, 187–193.

Schoenhals, M., Kassambara, A., De Vos, J., Hose, D., Moreaux, J., and Klein, B. (2009). Embryonic stem cell markers expression in cancers. Biochem. Biophys. Res. Commun. *383*, 157–162.

Schübeler, D. (2015). Function and information content of DNA methylation. Nature *517*, 321–326.

Shi, Y., Lan, F., Matson, C., Mulligan, P., Whetstine, J.R., Cole, P.A., Casero, R.A., and Shi, Y. (2004). Histone demethylation mediated by the nuclear amine oxidase homolog LSD1. Cell *119*, 941–953.

Shi, Y.J., Matson, C., Lan, F., Iwase, S., Baba, T., and Shi, Y. (2005). Regulation of LSD1 histone demethylase activity by its associated factors. Mol. Cell *19*, 857–864.

Speranzini, V., Ciossani, G., Marabelli, C., and Mattevi, A. (2017). Probing the interaction of the p53 C-terminal domain to the histone demethylase LSD1. Arch. Biochem. Biophys. *632*, 202–208.

Stovner, E.B., and Sætrom, P. (2019). epic2 efficiently finds diffuse domains in ChIP-seq data. Bioinformatics *35*, 4392–4393.

Taberlay, P.C., Statham, A.L., Kelly, T.K., Clark, S.J., and Jones, P.A. (2014). Reconfiguration of nucleosome-depleted regions at distal regulatory elements accompanies DNA methylation of enhancers and insulators in cancer. Genome Res. *24*, 1421–1432.

Tierling, S., Schmitt, B., and Walter, J. (2018). Comprehensive Evaluation of Commercial Bisulfite-Based DNA Methylation Kits and Development of an Alternative Protocol With Improved Conversion Performance. Genet Epigenet, *10*, 1179237X18766097.

van den Berg, D.L.C., Snoek, T., Mullin, N.P., Yates, A., Bezstarosti, K., Demmers, J., Chambers, I., and Poot, R.A. (2010). An Oct4-centered protein interaction network in embryonic stem cells. Cell Stem Cell *6*, 369–381.

Vinyard, M.E., Su, C., Siegenfeld, A.P., Waterbury, A.L., Freedy, A.M., Gosavi, P.M., Park, Y., Kwan, E.E., Senzer, B.D., Doench, J.G., et al. (2019). CRISPR-suppressor scanning reveals a nonenzymatic role of LSD1 in AML. Nat. Chem. Biol. *15*, 529–539.

Wang, Z., Zang, C., Rosenfeld, J.A., Schones, D.E., Barski, A., Cuddapah, S., Cui, K., Roh, T.-Y., Peng, W., Zhang, M.Q., and Zhao, K. (2008). Combinatorial patterns of histone acetylations and methylations in the human genome. Nat. Genet. *40*, 897–903.

Wang, J., Hevi, S., Kurash, J.K., Lei, H., Gay, F., Bajko, J., Su, H., Sun, W., Chang, H., Xu, G., et al. (2009a). The lysine demethylase LSD1 (KDM1) is required for maintenance of global DNA methylation. Nat. Genet. *41*, 125–129.

Wang, Y., Zhang, H., Chen, Y., Sun, Y., Yang, F., Yu, W., Liang, J., Sun, L., Yang, X., Shi, L., et al. (2009b). LSD1 is a subunit of the NuRD complex and targets the metastasis programs in breast cancer. Cell *138*, 660–672.

Wang, X.Q., Ongkeko, W.M., Chen, L., Yang, Z.F., Lu, P., Chen, K.K., Lopez, J.P., Poon, R.T., and Fan, S.T. (2010). Octamer 4 (Oct4) mediates chemotherapeutic drug resistance in liver cancer cells through a potential Oct4-AKT-ATP-binding cassette G2 pathway. Hepatology *52*, 528–539.

Wang, Y.D., Cai, N., Wu, X.L., Cao, H.Z., Xie, L.L., and Zheng, P.S. (2013). OCT4 promotes tumorigenesis and inhibits apoptosis of cervical cancer cells by miR-125b/BAK1 pathway. Cell Death Dis. *4*, e760.

Wang, J., Telese, F., Tan, Y., Li, W., Jin, C., He, X., Basnet, H., Ma, Q., Merkurjev, D., Zhu, X., et al. (2015a). LSD1n is an H4K20 demethylase regulating

memory formation via transcriptional elongation control. Nat. Neurosci. *18*, 1256–1264.

Wang, S., Lv, J., Zhang, L., Dou, J., Sun, Y., Li, X., Fu, X., Dou, H., Mao, J., Hu, X., and Bao, Z. (2015b). MethylRAD: a simple and scalable method for genome-wide DNA methylation profiling using methylation-dependent restriction enzymes. Open Biol. *5*, 5.

Wang, C., Lee, J.E., Lai, B., Macfarlan, T.S., Xu, S., Zhuang, L., Liu, C., Peng, W., and Ge, K. (2016). Enhancer priming by H3K4 methyltransferase MLL4 controls cell fate transition. Proc. Natl. Acad. Sci. USA *113*, 11871–11876.

Wang, S.P., Tang, Z., Chen, C.W., Shimada, M., Koche, R.P., Wang, L.H., Nakadai, T., Chramiec, A., Krivtsov, A.V., Armstrong, S.A., and Roeder, R.G. (2017). A UTX-MLL4-p300 Transcriptional Regulatory Network Coordinately Shapes Active Enhancer Landscapes for Eliciting Transcription. Mol Cell, *67*, 308–321 e6.

Wei, F., Schöler, H.R., and Atchison, M.L. (2007). Sumoylation of Oct4 enhances its stability, DNA binding, and transactivation. J. Biol. Chem. *282*, 21551–21560.

Wen, J., Park, J.Y., Park, K.H., Chung, H.W., Bang, S., Park, S.W., and Song, S.Y. (2010). Oct4 and Nanog expression is associated with early stages of pancreatic carcinogenesis. Pancreas *39*, 622–626.

Whyte, W.A., Bilodeau, S., Orlando, D.A., Hoke, H.A., Frampton, G.M., Foster, C.T., Cowley, S.M., and Young, R.A. (2012). Enhancer decommissioning by LSD1 during embryonic stem cell differentiation. Nature *482*, 221–225.

Yang, F., Zhang, J., and Yang, H. (2018). OCT4, SOX2, and NANOG positive expression correlates with poor differentiation, advanced disease stages, and worse overall survival in HER2^{+} breast cancer patients. OncoTargets Ther. *11*, 7873–7881.

Yegnasubramanian, S., Wu, Z., Haffner, M.C., Esopi, D., Aryee, M.J., Badrinath, R., He, T.L., Morgan, J.D., Carvalho, B., Zheng, Q., et al. (2011). Chromosome-wide mapping of DNA methylation patterns in normal and malignant prostate cells reveals pervasive methylation of gene-associated and conserved intergenic sequences. BMC Genomics *12*, 313.

Yu, G., Wang, L.G., and He, Q.Y. (2015a). ChIPseeker: an R/Bioconductor package for ChIP peak annotation, comparison and visualization. Bioinformatics *31*, 2382–2383.

Yu, Z., Xiao, Q., Zhao, L., Ren, J., Bai, X., Sun, M., Wu, H., Liu, X., Song, Z., Yan, Y., et al. (2015b). DNA methyltransferase 1/3a overexpression in sporadic breast cancer is associated with reduced expression of estrogen receptor-alpha/breast cancer susceptibility gene 1 and poor prognosis. Mol. Carcinog. *54*, 707–719.

Zaret, K.S., and Carroll, J.S. (2011). Pioneer transcription factors: establishing competence for gene expression. Genes Dev. *25*, 2227–2241.

Zentner, G.E., Tesar, P.J., and Scacheri, P.C. (2011). Epigenetic signatures distinguish multiple classes of enhancers with distinct cellular functions. Genome Res. *21*, 1273–1283.

Zhang, X., Lu, F., Wang, J., Yin, F., Xu, Z., Qi, D., Wu, X., Cao, Y., Liang, W., Liu, Y., et al. (2013). Pluripotent stem cell protein Sox2 confers sensitivity to LSD1 inhibition in cancer cells. Cell Rep. *5*, 445–457.

Zhao, H., Sun, Z., Wang, J., Huang, H., Kocher, J.P., and Wang, L. (2014). CrossMap: a versatile tool for coordinate conversion between genome assemblies. Bioinformatics *30*, 1006–1007.

Zheng, Y., Cohen-Karni, D., Xu, D., Chin, H.G., Wilson, G., Pradhan, S., and Roberts, R.J. (2010). A unique family of Mrr-like modification-dependent restriction endonucleases. Nucleic Acids Res. *38*, 5527–5534.

Zhu, B., Liu, T., Hu, X., and Wang, G. (2013a). Developmental toxicity of 3,4-dichloroaniline on rare minnow (Gobiocypris rarus) embryos and larvae. Chemosphere *90*, 1132–1139.

Zhu, Y., Sun, L., Chen, Z., Whitaker, J.W., Wang, T., and Wang, W. (2013b). Predicting enhancer transcription and activity from chromatin modifications. Nucleic Acids Res. *41*, 10032–10043.

Zibetti, C., Adamo, A., Binda, C., Forneris, F., Toffolo, E., Verpelli, C., Ginelli, E., Mattevi, A., Sala, C., and Battaglioli, E. (2010). Alternative splicing of the histone demethylase LSD1/KDM1 contributes to the modulation of neurite morphogenesis in the mammalian nervous system. J. Neurosci. *30*, 2521–2532.

STAR★METHODS

KEY RESOURCES TABLE

REAGENT or RESOURCE	SOURCE	IDENTIFIER
Antibodies		
anti-cMyc antibody	R and D Systems	Cat# MABE282, RRID:AB_11204521
anti-SSEA-1	R and D Systems	Cat# MAB430, RRID:AB_2208782
and AlexaFluor 555 nm	Molecular Probes	Cat# A-21422, RRID:AB_141822
anti-Oct4	Abcam	Cat# ab181557, RRID:AB_2687916
anti-CHD4	Abcam	Cat# ab72418, RRID:AB_1268107
anti-HDAC1	Abcam	Cat# ab7028, RRID:AB_305705
anti-Lsd1	Abcam	Cat# ab17721, RRID:AB_443964
anti-HBO1	Abcam	Cat# ab124993, RRID:AB_11001813
anti-Oct4	Santa Cruz Biotechnology	Cat# sc-8628, RRID:AB_653551
anti-H3K4me2	Abcam	Cat# ab32356, RRID:AB_732924
anti- H3K27Ac	Abcam	Cat# ab4729, RRID:AB_2118291
anti-H3K4me1	Abcam	Cat# ab8895, RRID:AB_306847
anti-H3K27me3	Abcam	Cat# ab6002, RRID:AB_305237
anti-β Actin	Santa Cruz Biotechnology	Cat# sc-47778 HRP, RRID:AB_2714189
Anti-Rabbit IgG	Jackson ImmunoResearch Labs	Cat# 111-035-003, RRID:AB_2313567
Anti- Mouse IgG	Jackson ImmunoResearch Labs	Cat# 115-035-003, RRID:AB_10015289
Biological Samples		
pCAG-Myc-Oct4	Addgene	13460
Chemicals, Peptides, and Recombinant Proteins		
TRIzol	Invitrogen	15596026
*Fsp*EI	NEB	
Protein A magnetic beads	Life Technologies	10002D
Protein G magnetic beads	Life Technologies	10004D
RNase	Roche	11119915001
Proteinase K	Worthington	LS004222
Quick-RNA™ MiniPrep Plus Kit	ZymoReseach	R1057
Verso One-Step RT-qPCR kit	Thermo Scientific	AB-4104A
Alkaline phosphatase staining kit	Sigma	AB0300
GST-Lsd1	Sigma	SRP0122
Oct4	Abcam	ab134876
Oct4	Abcam	ab169842
Bulk Histones	Sigma	H9250
EpiTect Fast Bisulfite Conversion Kit	QIAGEN	59802
Lipofectamine 2000	Thermofischer	11668019
Critical Commercial Assays		
Epigenase™ kit	Epigentek	P-0379
Deposited Data		
Raw and analyzed data	This paper	GSE135225
Experimental Models: Cell Lines		
P19 embryonal carcinoma cells	ATCC	CRL-182
F9 embryonal carcinoma cells	ATCC	CRL-1720
E14Tg2A Embryonic stem cells	MMRRC	015890-UCD
Oligonucleotides		
List of primers used	This paper	Table S4

(*Continued on next page*)

REAGENT or RESOURCE	SOURCE	IDENTIFIER
Software and Algorithms		
Trimmomatic v 0.36	Bolger et al., 2014	https://github.com/timflutre/trimmomatic
Bowtie2 v.2.3.3	Langmead and Salzberg, 2012	http://bowtie-bio.sourceforge.net/bowtie2/manual.shtml
Cutadapt v 2.2	Martin, 2011	https://cutadapt.readthedocs.io/en/stable/installation.html
ENSEMBL *Mus musculus* reference genome version GRCm38.93	GRCm38.p2 (Genome Reference Consortium Mouse Reference 38), INSDC Assembly GCA_000001635.4, Jan 2012	ftp://ftp.ensembl.org/pub/release-98/fasta/mus_musculus/dna/
Custom python scripts		https://github.com/natallah/methylRad
Bismark v 0.18.2	Krueger and Andrews, 2011	https://www.bioinformatics.babraham.ac.uk/projects/bismark/
BEDTools v 2.29.0	Quinlan and Hall, 2010	https://bedtools.readthedocs.io/en/latest/
Enhancer Atlas v 2.0	Gao and Qian, 2019	http://enhanceratlas.org/
TrimGalore v 0.6.4	Krueger, 2012	https://www.bioinformatics.babraham.ac.uk/projects/trim_galore/
epic2 2019-Jan-03	Stovner and Sætrom, 2019	https://bioepic.readthedocs.io/en/latest/
FastQC v. 0.11.7	Andrews, 2010	https://www.bioinformatics.babraham.ac.uk/projects/fastqc/
ChIPseeker v 1.22.0	Yu et al., 2015a.	https://bioconductor.org/packages/release/bioc/html/ChIPseeker.html
Ingenuity Pathway Analysis (IPA)	QIAGEN	https://www.qiagenbioinformatics.com/products/ingenuity-pathway-analysis/?gclid=Cj0KCQiAuefvBRDXARIsAFEOQ9GUaRrR3QZy42lJtb5QHvlHsmCrtw5fOeyRo0d2GEgfWxKTIPwd8w8aArVwEALw_wcB

LEAD CONTACT AND MATERIALS AVAILABILITY

Further information and requests for resources and reagents should be directed to and will be fulfilled by the Lead Contact, Humaira Gowher (hgowher@purdue.edu)

All unique/stable reagents generated in this study will be made available on request but we may require a payment for processing and shipping and/or a completed Materials Transfer Agreement if there is potential for commercial application.

EXPERIMENTAL MODEL AND SUBJECT DETAILS

F9 embryonal carcinoma cells (F9 ECCs), P19 embryonal carcinoma cells (P19 ECCs), and E14Tg2A Embryonic stem cells (ESCs) were cultured and maintained in gelatin-coated tissue culture plates. All three above cell lines are male. Differentiation of ECCs was induced by plating $20X10^6$ cells in low attachment 15 cm Petri dishes and the addition of 1μM Retinoic acid (RA). ESCs were differentiated by the same method with a concurrent withdrawal of LIF. The medium was replenished every two days and samples were collected on Days 4 and 8 post-differentiation.

Plasmids expressing Myc-Dnmt3a2 and FLAG-Lsd1 WT were transfected into F9 ECCs using Lipofectamine 2000. One day post-transfection, a UD sample was collected (D0), and transfected cells were induced to differentiate on gelatinized plates by the addition of RA. The next day, differentiated cells were trypsinized and plated on low adherence Petri dishes. Samples were collected on Days 4 and 8 post-differentiation. Lsd1 inhibitor treatment was performed as described 6 hr prior to induction of differentiation (Petell et al., 2016).

P19 ECCs were transfected with pCAG-Myc-Oct4 (Addgene 13460) using Lipofectamine 2000 per the manufacturer's instructions. Transfected cells were clonally propagated, and Myc-Oct4 expression was determined by western blots with anti-cMyc antibody (Millipore, MABE282).

METHOD DETAILS

DNA methylation analysis

Bisulfite sequencing: Bisulfite conversion was performed using an EpiTect Fast Bisulfite Conversion Kit (QIAGEN, 59802) according to the manufacturer's protocol. PCR conditions for outer and inner amplifications were performed (Petell et al., 2016). The pooled

samples were sequenced using NGS on a Wide-Seq platform. The reads were assembled and analyzed by Bismark and Bowtie2. Methylated and unmethylated CpGs for each target were quantified, averaged, and presented as percent CpG methylation. Number of CpGs for regions tested are listed in Table S1. Total number of reads used to calculate percent CpG methylation are listed in Tables S2 and S3. Primer sequences can be found in Table S4.

MethylRAD sequencing: Genomic DNA was isolated using a standard phenol:chloroform extraction, followed by ethanol precipitation. DNA from various samples was digested with *Fsp*EI for 4 hr at 37°C and subjected to electrophoresis through a 2% agarose gel. 30 base pair fragments were cut out, purified, and adaptors were ligated at 4°C overnight (Wang et al., 2015b). The ligated DNA was PCR amplified with index primers and sequenced using a Novaseq 6000. The primers used for PCR amplification is in Table S4. The details of the bioinformatics analysis of data are listed below.

Chromatin Immunoprecipitation and ChIP-Seq

ChIP was performed as described (Petell et al., 2016). Chromatin was sheared by sonication using a Covaris E210 device, according to the manufacturer's protocol. A total of 8μg of sheared crosslinked chromatin was incubated with 8μg of antibody pre-loaded on a 1:1 ratio of protein A and protein G magnetic beads (Life Technologies, 10002D and 10004D, respectively). After washing the beads, the samples were eluted in 1% SDS, 10 mM EDTA, 50 mM Tris-HCl, pH 8.0. Crosslinking was reversed by incubation at 65°C for 30 min with shaking. Samples were treated with RNase (Roche, 11119915001) for 2 h at 37°C, and subsequently treated with Proteinase K (Worthington, LS004222) for 2 h at 55°C. DNA was purified by phenol:chloroform extraction followed by ethanol precipitation and quantified using PicoGreen (Life Technologies, P11495) and NanoDrop 3300 fluorospectrometer. qPCR was then performed using equal amounts of IN and IP samples. Fold enrichment was first calculated as: $2\char`\^(C_t(IN)-C_t(IP))$. Percent enrichment = Fold enrichment X 100. Significance of change was determined via *p-value*, which was calculated by GraphPad Prism using Student's t test.

Table S4 lists sequences of primers used.

Gene expression analysis

RNA was isolated using the TRIzol reagent (Invitrogen, 15596026) according to the manufacturer's protocol. Samples were treated with DNase (Roche, 04716728001) at 37°C, and then purified using a Quick-RNA™ MiniPrep Plus Kit (ZymoReseach, R1057). Reverse-transcription quantitative PCR was performed by using Verso One-Step RT-qPCR kits (Thermo Scientific, AB-4104A) with 1μg of purified RNA. Gene expression was calculated as ΔC_t which is $C_t(Gene)- C_t(Gapdh)$. Change in gene expression is reported as fold change relative to that in undifferentiated cells, which was set to 1. See Table S4 for primers used.

Microscopy

Bright field images of embryoid bodies (EBs) were obtained with Zeiss microscope using a 10X objective. Alkaline phosphatase staining was performed using solutions supplied by an alkaline phosphatase staining kit (Sigma, AB0300). Cells were cross-linked with 1% formaldehyde for 5 min, followed by quenching with a final concentration of 150 mM glycine. Cells were washed twice with 1xPBS, then twice with combined staining solution (BCIP and NBT). The stain was developed in the dark for 5 min, then washed three times with 1XPBS. SSEA-1 immunofluorescence was performed using the following antibodies: anti-SSEA-1 (Millipore, MAB430) and AlexaFluor 555 nm (Life Technologies, A21422). SSEA-1 and Alkaline phosphatase staining were imaged using 20X objectives under Nikon Ts and Zeiss microscopes, respectively.

Co-precipitation assays

For co-immunoprecipitation (Co-IP), the nuclear extract was prepared according to manufacturer's protocol (Active Motif, 40010) except that DNase was added for the release of chromatin-associated proteins. The Co-IP was performed using 1:1 mix of Dynabeads Protein A (Life Technologies, 1002D) and Dynabeads Protein G (Life Technologies, 1004D), and conjugated with 5 μg antibody and with 50 μg of nuclear extract according to the manufacturer's protocol. Antibodies used include: anti-Oct4 (Abcam, ab181557), anti-CHD4 (Abcam, ab72418), anti-HDAC1 (Abcam, ab7028), anti-Lsd1 (Abcam, ab17721) and anti-HBO1 (Abcam, ab124993).

Pull down assays were performed using 1 μg of GST-Lsd1 (Sigma, SRP0122) incubated with 1 μg of recombinant Oct4 (abcam, ab134876) and Glutathione Sepharose 4B (GE healthcare, 17-0756-01) resin in the binding buffer (50 mM Tris pH 8.5, 50 mM KCl, 5 mM MgCl, 0.5% BSA, and 5% glycerol, complemented with a cocktail of protease inhibitors) overnight at 4°C with gentle agitation. The resin was washed twice with binding buffer and proteins were eluted using the elution buffer (50 mM Tris-HCl, 10 mM reduced glutathione, pH 8) according to the manufacturer's instructions. Eluate and input were loaded onto a 10% SDS-PAGE gels and blots were probed using anti-Lsd1 (Abcam, ab17721) and anti-Oct4 (Santa Cruz, sc-8628) antibodies.

In vitro Lsd1 demethylase activity assay

An *in vitro* fluorometric assay was used to detect Lsd1 demethylase activity using an Epigenase™ kit (Epigentek, P-0379) according to the manufacturer's protocol. 0.25 μM of Lsd1 (Sigma, SRP0122) was used for activity assays together with 0.5 μM (or as indicated) of Oct4 (abcam, ab134876 and ab169842) or BSA (Sigma, A3059) or the catalytic domain of Dnmt3a (*purified in-house*) or 0.1 mM of the Lsd1 inhibitor Tranylcypromine (TCP). Signals were measured using a CLARIOstar plate reader and analyzed using MARs software as described by the manufacturer.

Histone demethylation assay

Lsd1 histone demethylation assays were performed as described (Shi et al., 2004). A total of 30 μg of bulk histones (Sigma, H9250) in a histone demethylation buffer (50 mM Tris pH 8.5, 50 mM KCl, 5 mM MgCl, 0.5% BSA, and 5% glycerol) were incubated with 0.25 μM of Lsd1 (Sigma, SRP0122) alone, or increasing concentrations (0.125 μM, 0.25 μM, 0.5 μM, 1 μM) of Oct4 (Abcam, ab134876 and ab169842), or 0.1 μM TCP for 4 hr at 37°C. Lsd1 activity was monitored by western blot using anti-H3K4me2 antibody (Abcam, ab32356). The membrane was stained by Ponceau S to determine equal loading of the reaction mix.

Co-immunoprecipitation

Co-immunoprecipitation experiments was also performed as described (Whyte et al., 2012). Briefly, undifferentiated F9 ECCs and ESCs were washed and harvested in cold 1X PBS. Cellular proteins were extracted using TNEN250 lysis buffer (50 mM Tris pH 7.5, 5 mM EDTA, 250 mM NaCl, 0.1% NP-40) complemented with protease inhibitors at 4°C with rotation for 30 min. Complexes were then immunoprecipitated overnight at 4°C with rotation by incubating the supernatant solution supplemented with two volumes of TNENG (50 mM Tris pH 7.5, 5 mM EDTA, 100 mM NaCl, 0.1% NP-40, 10% glycerol) with Dynabeads® M280 (Life Technologies, 11203D) bound to 5 ug of antibody. Beads were washed with TNEN125 (50 mM Tris pH 7.5, 5 mM EDTA, 125 mM NaCl, 0.1% NP-40) and samples were eluted by boiling for 10 min in Laemmli's loading buffer containing 100 mM DTT. Western blots were performed with NuPAGE 4%–12% Tris-Bis gels. Antibodies used included: Lsd1 (abcam, ab17721), HDAC1 (abcam, ab7028), Mi-2b (abcam, ab72418).

Western blot

Western blot analysis was performed using the standard method and the following antibodies and dilutions: anti-Dnmt3a, 1:1000 (Active Motif, 39206), Anti-Lsd1, 1:1000 (abcam, ab17721) and anti-β Actin, 1:1000 (Santa Cruz, sc8628), and anti-Rabbit, 1:10,000 (Jackson Immunoresearch, 111-035-003) or anti-Mouse, 1:10,000 (Jackson Immunoresearch, 115-035-003). Chemiluminescence was performed according to the manufacturer's protocol (Thermo-Fisher Scientific, 34580).

MethylRAD sequencing Analysis

Alignment and Quality Control

A total of 258,987,008 single end 1x150 sequencing was performed using a NovaSeq 6000 platform for undifferentiated and day 4 F9 samples. The program FastQC v. 0.11.7 (Andrews, 2010) was used to check data quality pre- and post-quality trimming/adaptor removal. Adapters were removed from reads using Trimmomatic v. 0.36 (Bolger et al., 2014). Trimmomatic is a program that removes adaptor sequences and trims short Illumina reads based on quality. Cutadapt version 2.2 (Martin, 2011) was used to trim reads further, removing the first two and last two bases of each read. Reads containing greater than 0 N's were discarded. After trimming, a total of 112,289,569 reads remained in the undifferentiated and day 4 samples. Reads which do not have *Fsp*E1 sites present anywhere in the read were removed using 'grep', leaving a total of 71,730,977 reads. Finally, Bowtie2 version 2.3.3 (Langmead et al., 2009; Langmead and Salzberg, 2012) was used to map reads to the ENSEMBL *Mus musculus* reference genome version GRCm38.93. A maximum of 1 mismatch was allowed in read mapping. The mapping rate of reads was 89%, with 64% of the reads mapped to the genome exactly 1 time and included in further analyses.

Data preprocessing

Methylated sites were cataloged by iterating through all read sequences to find a matched pattern of methylation (i.e., CCGG, CCAGG, and CCTGG) and recording its location in the genome. The number of reads mapping to each methylated site was recorded and adjusted for substitution, deletion, and insertion accordingly. Sites were also matched with the reference genome for verification. Sites that had less than 5 reads were removed from downstream analysis; counts from duplicate sites between patterns were summed as one site. Python and R scripts used in this analysis are included at https://www.github.com/natallah.

Annotation to LSD1 Enhancers

Sites in the LSD1 enhancers were modified to include 1 kb up- and downstream of the identified start site. Both the undifferentiated and day 4 differentiated F9 samples were annotated to the modified LSD1 regions using BEDTools intersect. The total amount of methylation in a region was determined by combining the read counts of all sites in that region. Upper and lower quartiles were used in thresholding regions as gaining or losing methylation. Specifically, all regions with at least 22 counts more in undifferentiated than in day 4 differentiated samples were identified as losing DNA methylation as differentiation occurred. All regions with at least 30 counts more in day 4 samples than in undifferentiated samples were identified as gaining DNA methylation.

Quantifying methylated regions

The union of enhancers found in both the undifferentiated and day 4 differentiated F9 samples were determined. The difference in methylation for each combined enhancer regions were computed by subtracting the total methylation in day 4 differentiated F9 samples to that of the undifferentiated sample. Comparative figures were produced from these final data.

Determining methylation level of enhancers

DNA sequences of all known enhancers for the ESC_J1 strain of mouse were downloaded from EnhancerAtlas V2.0 (Gao et al., 2016). Overlaps between MethylRAD sites and enhancers were found using BEDTools intersect. Reads that overlapped the enhancer for the same gene were then summed together. Raw counts were normalized for length. The average length of enhancers in the EnhancerAtlast database was computed for each gene. If different studies in the database reported variable lengths for enhancers, the

average length of the enhancer was computed. Counts for each sample were then divided by the length of the enhancer and subsequently multiplied by 1000 (to enhance readability). The 25th and 75th percentiles were computed for all enhancers separately for undifferentiated and day four samples and were used as cutoffs for low and intermediate methylation. Thus, for undifferentiated samples, enhancers annotated as having low methylation have normalized counts between (0, 24.57], intermediate methylation are between (24.57, 243.68], and high methylation have greater than 243.58 normalized counts. Enhancers in day 4 samples are annotated as highly methylated if normalized counts are observed to be between (0, 24.06], intermediate counts are between (24.06, 256.56], and high counts have greater than 256.56 normalized counts.

ChIP-Seq Analysis
Quality Control and Mapping
Sequencing was performed using a NovaSeq 6000 to generate > 80 million paired-end (2x50) reads (> 80 million) undifferentiated and day 4 F9 samples. Sequence data quality was determined using FastQC software (Andrews, 2010) and quality based trimming and filtering (minimum quality score 30 and minimum read-length 20) was performed through TrimGalore tool (Krueger, 2012). Greater than 95% of the reads from all samples were retained after quality control and were used for the mapping. Mapping was performed against the mouse reference genome (GRCm38) using Bowtie2 (Langmead and Salzberg, 2012) with a maximum of 1 mismatch. The overall mapping rate was > 97% for all samples. Bowtie2 derived BAM files were further filtered to retain the reads with minimum MAPping Quality (MAPQ) 10.
Peak-calling
Peak calling was performed using epic2 (Stovner and Sætrom, 2019) for each Input-ChIP pair using the mouse reference genome (GRCm38). The tool was run with MAPQ10 filtered BAM files and the default parameters (–falsediscovery-rate-cutoff 0.05,–binsize 200).
Peak-annotation
Peak-annotation and visualization was performed with R-package ChIPseeker (Yu et al., 2015a). Annotations were performed for all epic2 peaks called with default parameters.
Overlap of H3K4me1 peaks in F9 ECCs with those in ESCs
Overlapping LSD1 bound sites between H3K4me1 peaks in F9 ECCs and ESCs (Whyte et al., 2012). Correct overlap, was determined by converting peak coordinates from mm9 to mm10 using CrossMap tool (Zhao et al., 2014).

Pathway Analysis
IPA (Ingenuity Pathway Analysis), (IPA, QIAGEN Redwood City, https://www.qiagen.com/ingenuity), was used in the annotation of genes and in performing the pathway analyses.

QUANTIFICATION AND STATISTICAL ANALYSIS

methylRAD statistical analyses and software
Methods are described in the section entitled "DNA methylation is not established at PpGe during F9 ECC differentiation," and also in the Method Details section entitled "MethylRAD sequencing Analysis." -fastQC version 0.11.7 was used to check data quality before and after filtering.

Read trimming was performed using Trimmomatic v. 0.36 to remove Illumina adaptor sequences from reads. Reads containing greater than 0 N's were discarded.

Cutadapt v 2.2 was used to remove the first two and last two bases of each read. -grep "CCGG|GGCC|CCAGG|GGTCC|CCTGG" *fastq > sites.fastq was used to keep only reads with FspEI sites present

Bowtie v2.3.3 was used to map reads to the GRCm38.93 Mus Muscusus genome, removing all reads with more than 1 mismatch

Methylated sites were identified and methylation events counted using a custom Python script, which is available at https://www.github.com/natallah

A total of 1,370,254 cytosines were captured genome-wide with a cutoff of 5 reads per site minimum (1,370,254 cytosines had at least 5 reads aligned with Bowtie2). The difference in methylation was calculated by summing reads which overlap with enhancer downloaded from EnhancerAtlas 2.0.

Differences were calculated between differentiated and undifferentiated samples by calculating the difference $d = x_{ij}-x_{ij}$ with x equivalent to the read count (total raw reads) for enhancer i in sample j. Undifferentiated enhancer read counts were subtracted from differentiated enhancer counts. Special focus was given to the enhancers which were identified as Lsd1 bound previously (Whyte et al., 2012). Low-intermediate-high levels of methylation were calculated using the total read counts in all enhancers from the EnhancerAtlas by using the 75th percentile as the lower bound for high methylation levels and the 25th percentile as the upper bound for low methylation levels.

BEDtools overlap was used to identify reads overlapping with specific genomic features (enhancers, Lsd1 bound enhancers, promotors)

ChIPseeker v 1.22.0 was used to annotate site distribution across the genome.

ChIP-seq statistical analyses and software

Methods are described in the section entitled "High throughput analysis of changes in H3K4me1 at PpGe" as well as in the section entitled "ChIP-Seq Analysis."

FastQC v 0.11.7 was used to check read quality before and after read trimming.

Bowtie2 v 2.3.3 was used to map to the mouse reference genome version GRCm38, removing alignments with greater than 1 mismatch. Reads with less than a MAPQ of 10 were removed.

TrimGalore v 0.6.4 was used to trim adaptor sequences and remove reads with under a read-length of 20 and with less than a quality PHRED score of 30.

Peak calling was performed using Epic2 v 2019-Jan-03 with all defaults on each IP and input pair. The peaks were filtered selecting only peaks with false discovery rate less than or equal to 5% and with greater than or equal to a log fold-change (IP/input control) of 2.–binsize was set to 200 in epic2.

Peaks which had greater than a z-score of 1 were counted as increased, while those with below a z-score of −1 were counted as decreased. The peaks with a z-score greater than or equal to −1 and less than or equal to 1 were annotated as not changing (see Figure 4). Z-score was calculated as how many standard deviations a certain value is above or below the mean using formulae $z = (x − μ) / σ$, where x corresponds to difference between log2FC of D4 and undifferentiated samples for a specific gene, μ is mean difference across all genes, and σ is standard deviation of difference across all genes.

Pathway analyses

All pathway analyses were performed using Ingenuity Pathway analysis (IPA), as described in the section entitled "DNA methylation is not established at PpGe during F9 ECC differentiation," as well as the Supplemental section entitled "Pathway Analysis" using *Mus musculus* as the organism, and input as genes which are low (less than or equal to the 25th percentile methylation), intermediate (greater than the 25th percentile and less than the 75th percentile for all enhancers from EnhancerAtas 2.0), or high (greater than or equal to 75th percentile methylation).

A one-tailed Fisher's exact test was used to calculate functional enrichment, and all p values were adjusted for multiple testing using the Benjamini-Hochberg method. The adjusted p value cutoff for significance is padj < 0.05.-ggplot was used to generate pie charts, waterfall plots, and bar charts.

DATA AND CODE AVAILABILITY

The datasets generated during this study are available at GEO under accession GSE135225 (ChIP-seq) and GSE135226 (methylRAD-seq). ChIP-seq peak annotations and genome browser track files are included.

All code and scripts use to analyze data and to generate genomic plots are at https://www.github.com/natallah.